Pilot allocation in downlink for cell-free communication systems

Wafa Haj Hmida

Thèse de doctorat

Université de Limoges

Université de Limoges

ED 610 - Sciences et Ingénierie des Systèmes, Mathématiques, Informatique (SISMI)

XLIM: Systèmes & Réseaux intelligents

Laboratoire SYSCOM, ENIT

Thèse pour obtenir le grade de

Docteur de l'Université de Limoges

Discipline: Sciences et technologies de l'information et de la communication

Présentée et soutenue par

Wafa HAJ HMIDA

Intitulée

Affectation de pilotes dans la liaison descendante des systèmes de télécommunication sans cellule

Soutenue le 17 décembre 2020

Thèse dirigée par:

*M. **Ammar BOUALLEGUE**, Professeur Emérite, Ecole Nationale d'Ingénieurs de Tunis*

*M. **Vahid MEGHDADI**, Professeur, Université de Limoges France*

JURY:

Président du jury

*M. **Rabah ATTIA**, Professeur, Ecole Polytechnique de Tunisie*

Rapporteurs

*Mme **Fatma ABDELKEFI**, Maître de conférence-HDR, Ecole Supérieure des Communications de Tunis*

*M. **Guillaume FERRE**, Maître de conférence-HDR, Université de Bordeaux*

Examinateur

*M. **Jean Pierre CANCES**, Professeur, Université de Limoges France*

To the memory of my dear uncle Taoufik,
to my father and mother,
to Kawther, Slim, Achraf,
to my husband Ahmad,
to my future baby,
and to those who have inspired me.

Abstract

In Cell-Free massive Multiple-Input-Multiple-Output (Cell-Free massive MIMO) systems, we distribute in a coverage area a massive number of access points, mastered by central processing units (CPUs), to simultaneously serve much smaller number of user equipments (UEs) over the same time/frequency resources. In contrast to the centralized massive MIMO, cell-free massive MIMO is characterized by a channel hardening not sufficiently accentuated, thus, it will be appropriate to include downlink (DL) pilots to estimate the DL channel.

This thesis considers a DL pilot assignment for the cell-free massive MIMO systems by defining a metric, involving the inter-user interference (IUI). This metric gives insights about DL pilot contamination. A threshold is then defined to optimize the number of DL pilots, which maximizes the minimum per-user DL throughput. This approach gives a conflict graph, where each UE is regarded as a vertex of the graph. It consists in a combinatorial optimization problem that can be approximated using a graph coloring algorithm. It is a greedy algorithm whose steps are described as follows. By fixing the adequate threshold, maximizing the minimum per-user DL throughput, a conflict or interference graph is constructed. It models the potential interference among interfering UEs, the UEs between which there is an edge are in conflict, i.e., present a high IUI. Then, the proposed scheme mitigates the potential IUI by appointing *different* DL pilots to connected UEs with high IUI and *same* DL pilots to UEs with low IUI in the conflict graph in accordance with some coloring rules.

The simulation results validate that the minimum per-user DL throughput based on the proposed approach outperforms the conventional methods, i.e., statistical channel state information, the orthogonal and the random pilot assignment in the DL training. Our analysis underlines also the reduction of the DL pilot overhead ratio using the DL pilot assignment based on our proposed scheme, compared to the conventional methods aforementioned.

Keywords: Cell-Free massive MIMO, downlink (DL) training, conjugate beamforming, DL pilot contamination, pilot overhead, per-user DL throughput, channel hardening, DL pilot assignment, graph coloring.

Résumé

En systèmes « Cell-Free massive Multiple-Input-Multiple-Output (Cell-Free massive MIMO) » on distribue dans un territoire géographique un nombre massif de points d'accès, contrôlés par des unités centrales de processing (CPUs), afin de servir simultanément un nombre beaucoup moins inférieur au nombre d'équipements utilisateurs dans les mêmes ressources temporelles et fréquentielles. Contrairement aux systèmes MIMO massifs centralisés, « Cell-Free massive MIMO » est caractérisé par un durcissement de canal pas suffisamment accentué, c'est pourquoi il serait convenable d'inclure des pilotes envoyés en voie descendante afin d'estimer le canal descendant.

Cette thèse met en exergue l'allocation de pilotes en voie descendante en systèmes « cell-free massive MIMO » moyennant une métrique qui prend en compte l'interférence inter-utilisateurs en voie descendante. Cette métrique nous donne une information sur le taux de sévérité du problème de «contamination de pilotes envoyés en voie descendante ». Suite au calcul de cette métrique, un seuil d'interférence est défini pour déterminer les utilisateurs qui sont susceptibles de réutiliser le même pilote en voie descendante. Fixer un tel seuil vise à optimiser le nombre de pilotes envoyés en voie descendante, tout en maximisant le minimum du débit effectif par utilisateur en voie descendante. Cette approche donne lieu à un graphe de conflit, dans lequel chaque équipement utilisateur est considéré comme étant un nœud du graphe. C'est un problème d'optimisation combinatoire qui pourrait être résolu approximativement en utilisant un algorithme de coloriage. C'est un algorithme glouton dont les étapes sont les suivantes. En fixant un seuil adéquat, qui maximise le minimum du débit effectif en voie descendante par utilisateur, un graphe de conflit est ainsi construit. Il modélise l'interférence susceptible d'être présente parmi les équipements utilisateurs interférents, où chaque équipement utilisateur représente un nœud du graphe de conflit. Ensuite, la méthode de coloriage proposée permet de mitiger l'interférence inter-utilisateurs par l'affectation de *différents* pilotes en voie descendante aux équipements utilisateurs directement connectés dans le graphe de conflit, caractérisés par une interférence considérable et le *même* pilote aux utilisateurs, non directement connectés dans le graphe de conflit, présentent avec une interférence moins prédominante dans le graphe de conflit. Ce processus de coloriage s'effectue en accord à des règles bien déterminées.

Les résultats de simulation démontrent que la méthode proposée présente des performances, en termes de débit effectif par utilisateur en voie descendante, mieux que celles

des méthodes existantes à l'instar de la méthode celle qui s'appuie sur la connaissance de la statistique du canal « statistical channel state information », l'allocation orthogonale et aléatoire de pilotes en voie descendante. De surcroît, notre analyse met l'accent également sur la réduction de la charge de pilotes en voie descendante en utilisant l'allocation de pilotes en voie descendante reposant sur notre méthode proposée comparativement aux méthodes conventionnelles susmentionnés.

Mots clés: "Cell-Free Massive MIMO", phase d'apprentissage en voie descendante, "beamforming conjugué", contamination de pilotes en voie descendante, charge de pilotes débit effectif par utilisateur en voie descendante, durcissement de canal, allocation de pilotes en voie descendante, coloriage de graphe.

Acknowledgments

It is the long-awaited instant to deal with the acknowledgments part in my thesis. Here I am crossing the finish line with great pleasure. I have kept saying to myself: "I can make it even though it is late, for sure there is an exit, where there's a will, there's a way". If I am here, it is thanks to the help of many persons to handle the challenging phases of my thesis.

First and foremost, I would like to present my sincere thanks to the members of my thesis jury: Dr. Fatma ABDELKEFI and Dr. Guillaume FERRE, for accepting to be the reporters of my thesis, Pr. Jean Pierre CANCES and Pr. Rabah ATTIA to be the examiners. I'm sure that their remarks and suggestions will be so precious to pursue my research.

This project would not have turned from a mirage to a reality without the trust of my supervisor, Pr. Vahid MEGHDADI. I have the chance to work with such a reseacher with a nice combination of scientific rigor and good humor. He has a listening sense and has the art of asking pertinent questions, which have helped me to consolidate my reflexions about the thesis topic. He gave me very valuable guidelines and he was there for me when I needed advice. I'm very grateful to him for being very supportive personnally and professionally. He did not show me the path of my research axis but he taught me how to walk while "going from failure to failure without losing enthusiasm" and see the failure as an opportunity to grow gradually. I still remember his saying "it is not a failure, it is the process of exploration". He has pushed me forward and he has given me the desire to always go ahead to adjust in order to achieve some targets. Although I have worked with him most of the time remotely, but he was a great inspiration to me, I really learned a lot from him throughout the process of my thesis. He has all the qualities that make him a leader par excellence. I am really grateful to him to be a pleasant companion on my research adventure.

Furthermore, I'm grateful to my supervisor Pr. Ammar BOUALLEGUE for giving me the chance to do my PhD. I would like to thank him for being available to discuss my thesis progress, for his support and his advice. I'm grateful to him to make me love his course "Information Theory", this is where I got started in my domain. He developed in me more and more the sense of imagination to better assimilate the basic notions.

I would like to thank my research community members who didn't hesitate to re-

spond to my emails without even knowing me, Pr. Emil BJORNSON, Pr. Abdelhalim ZEKRI, Dr. Giovanni INTERNADO, Dr. Mahdi BARZEGAR, and Dr. Saeid HAGHIGHATSHOAR.

Big thanks are addressed to my friends for motivating me and for the great time. I would like to thank my sport coaches, Amir and Ayoub, for pushing my limits and to make me more and more resilient. Many thanks for those who have inspired me directly or indirectly.

I would like to express my infinite love and my gratitude to my family for having faith in me and for immeasurable support on all levels. My deepest gratitude is expressed to my parents for their deepest love and for their considerable effort to awaken in me the curiosity, to share a strong desire to study combining the useful with the pleasure. Particular attention shall be drawn to my brothers Achraf and Saleem and to my sister Kawther for their unconditional love, affection and encouragements. I would like to thank also my parents-in-law for their support.

Last but foremost, I would like to express my gratitude to my husband Ahmad for his love, his patience and his dedication to give me the strength to carry on my thesis. Thanks for being a lovely partner.

Table of contents

List of Figures

Notations and Acronyms

Mathematic notations

Boldface letters	denote column vectors.
$()^*$	stands for the conjugate.
$()^{\mathrm{H}}$	stands for the conjugate transpose.
$\mathbb{E}\{.\}$	expectation operator.
$z \sim \mathcal{CN}(\mu,\, \sigma^2)$	denotes a circularly symmetric complex Gaussian random variable (RV) z with mean μ and variance σ^2.

Acronyms

AP	**A**ccess **P**oint
BS	**B**ase **S**tation
CDF	**C**umulative **D**istribution **F**unction
CoMP	**Co**ordinated **M**ulti**P**oint
CSI	**C**hannel **S**tate **I**nformation
iCSI	**i**nstantaneous **CSI**
sCSI	**s**tatistical **CSI**
CPU	**C**entral **P**rocessing **U**nit
CF-mMIMO	**C**ell **F**ree massive MIMO
DL	**D**own **L**ink
GC-PA-CF-mMIMO	**G**raph **C**oloring based **P**ilot **A**ssignment in **C**ell-**F**ree **m**assive MIMO
ISD	**I**nter-**S**ite **D**istance
i.i.d	**i**ndependent, **i**dentically **d**istributed
MRC	**M**aximum **R**atio **C**ombining
MRT	**M**aximum-**R**atio **T**ransmission
MIMO	**M**ultiple **I**nputs **M**ultiple **O**utputs
SNR	**S**ignal-to- **N**oise **R**atio
UL	**U**p **L**ink
ZF	**Z**ero **F**orcing

Chapter 1

Introduction

> *If I had an hour to solve a problem, I'd spend 55 minutes thinking about the problem and 5 minutes thinking about solutions.*
>
> *Albert Einstein.*

Contents

1.1 Research context

Every new generation of wireless networks delivers faster speeds and more functionality to our phones. First, 1G brought us the first cellular network. Second, 2G let us text for the first time. Third, 3G brought us access to the internet and 4G delivered high speed of data. With the recent rise in the number of wireless devices and with the internet service, there is an amount of data crossing the network. As a consequence, 4G networks have just reached the limit of its capacity due to the rapid growth in rate, and the Quality of Service (QoS) demands. To this end, researchers have recourse to 5G, the next generation of wireless communication systems. It is able to handle 1000 times more traffic and it can be up to 10 times faster than 4G Long Term Evolution (LTE).
5G should offer high performance in terms of [1]:

- **Rate:** It is from 100 Mbps up to 1 Gbps per user equipment (UE);
- **Latency:** A low latency rate which is about 1 millisecond (ms);
- **Density of connection:** It is about 1 M connection/km^2.

Thanks to 5G, not only smartphones and laptops are connected to the internet but also objects such as connected cars. In fact, 5G will be the foundation for virtual reality, autonomous driving, and the Internet of things. Based on increasing the area throughput in cellular networks [2], whose formula can be divided up into three different terms, available spectrum, cell density and spectral efficiency, as follows

$$\underbrace{\text{Area throughput}}_{\text{bit/s/km}^2} = \underbrace{\text{Available spectrum}}_{\text{Hz}} \times \underbrace{\text{Cell density}}_{\text{Cell/km}^2} \times \underbrace{\text{Spectral efficiency}}_{\text{bit/s/Hz/ Cell}}. \tag{1.1}$$

To increase the area throughput, the three of its composed terms should be improved. To that end, there are 4 technologies emerging as pillars of 5G: millimeter waves (mmWaves), small cells, massive multiple-inputs multiple-outputs (MIMO), and beamforming. Making all of these systems work together will be a whole other challenge. Each of these 4 technologies will be explained as follows:

1. **MmWaves**: In 4G, the UEs use specific frequencies under 6 GHz on the radio frequency spectrum. But these frequencies are starting to get more crowded. As the number of UEs gets higher and higher, researchers are experimenting with broad-

casting on shorter mmWaves, having frequency between 30 GHz and 300 GHz. This section of spectrum is never been used before for mobile devices and opening it up means more bandwidth for every UE. According to communication principles, the higher the frequency of any waves is, the lesser the signal range is. So the mmWaves can't travel well through buildings or other obstacles and they tend to be absorbed by plants and rain. To overcome this problem of pathloss, small cells may be used.

2. **Small cells**: In 4G, wireless networks rely on large high powered cell towers to broadcast their signals over long distances. But higher frequency mmWaves are attenuated traveling through obstacles. Small cell networks would solve that problem using thousands of low-power mini BSs. These BSs would be much closer together than traditional towers forming a set of relays to transmit signals around obstacles.

3. **Massive MIMO**: In 4G, BSs have about a dozen ports for antennas that handle all cellular traffic. For mmWaves, as the frequency gets higher and higher, the wavelength of a signal gets shorter and shorter. Then, the antenna spacing decreases so that we can increase the number of antenna elements, getting a massive MIMO system. In such system, the BSs can support hundreds of antennas. This could increase the capacity of today's networks. Massive MIMO comes with its own complications, cellular antennas broadcast information in every direction at once and all of those crossing signals could cause serious interference. This brings us to beamforming technology.

4. **Beamforming**: In order to transmit data at multiple antennas in massive MIMO, precoding must be performed to facilitate data processing. Precisely, an antenna radiates electromagnetic waves in all directions isotropically. Owing to multiple antennas, precoding becomes relevant to direct the signal from the antenna array towards one or more intended receivers with an increased field strength, it is called "pencil beam forming" [3]. This precision prevents interference, that means the BSs could handle more data streams in UL and DL at once.

1.2 Motivation and problems description

1.2.1 Motivation

Among the pillars aforementioned of 5G, we focus on massive MIMO, where the base station (BS) can support a large number of antenna much larger than the number of user

equipments (UEs). The latters are served simultaneously in the same time-frequency resource. This could provide high throughput, reliability, and energy efficiency with simple signal processing [2,4,5]. The massive MIMO antennas in cellular networks can be deployed in centralized or distributed setups. Centralized or collocated massive MIMO, where all the antennas located in the same BS in the cell center, serve only UEs within that cell. This architecture confers an advantage of low backhaul requirements, but it suffers from inter-cell interference especially for UEs that are close to the cell boundaries [3].

In contrast, in distributed massive MIMO, the antennas are geographically deployed on a large space within the cell. It reduces inter-cell interference through a coherent cooperation between BSs via advanced backhaul. By exploiting diversity and cooperation, it offers much higher probability of coverage than colocated massive MIMO [6]. However, it comes with its own complications increasing backhaul requirements and deployment costs and it needs a performant central processing unit (CPU). In particular, the channel state information (CSI) must be shared among the BSs in distributed massive MIMO.

Recently, taking into consideration the problem of very high interference at the edge of a cell and the benefits of distributed massive MIMO, researchers point the compass direction arrow in other direction and deal with cell-free massive MIMO [7–9]. It is a particular deployment of distributed massive MIMO where a large number of access points (APs), equipped with single or multiple antennas, are located within an unlimited area (no cells). Fronthaul connections are involved to link the APs to CPUs, which are connected via backhaul network, if there are multiple CPUs. All APs serve coherently all UEs in the same time-frequency resource. More deeply, each AP applies beamforming, using local channel estimates resulting from received uplink (UL) pilots, to transmit data to the UEs. The APs cooperate with each other thanks to the CPUs. The latters are dedicated to collection and distribution of payload data, power control and pilot assignment [10]. In order to minimize the backhaul requirements, the CPU sends to the APs the data to be transmitted to the UEs and receives sufficient statistics of the received data-symbols from all the APs. It is to mention that neither the channel estimates, nor beamformers are forwarded to the CPU, they are computed locally at the APs [11]. In practice, we should notice a user-centric virtual-cell massive MIMO [12], which is a specific case of cell-free massive MIMO. Its specificity is that each UE is served only by a limited number of APs, requiring less backhaul overhead than the cell-free massive MIMO [13].

The benefits to opt for cell-free massive MIMO are:

(i) Improving spatial multiplexing: The spatial muliplexing is improved by increasing the macro-diversity gain, as each UE receives the same signal transmitted from APs situated in different sites by using channels with different characteristics. This ameliorates the autoimmunity against the shadow fading and the path-loss;

(ii) Reducing the inter-user interference (IUI): When we have a distributed topology, the APs are more likely closer to the UEs. This improves the quality of the channel estimation and, as a consequence, the accuracy of the beamforming. More directive and spatially focused beams result in less IUI in comparison with the centralized massive MIMO especially for cell-edge UEs, which suffer from a very high interference;

(iii) Offering a very high coverage probability and improving energy efficiency [6].

However, this comes at the price of higher fronthaul requirements and the need for distributed signal processing. Moreover, another feature characterising the cell-free massive MIMO is its low degree of *channel hardening* [14–16].

The channel hardening phenomenon makes the fading channel be as determinist, i.e., it behaves as if it were a non fading channel and the random fluctuations are still there but its impact on the communication is negligible. In conventional massive MIMO, the channel hardening eliminates the impact of small-scale fading owing to the high spatial diversity. The channel variations tend to be near to the channel statistical characterization, i.e., the channel hardens more and more, when the number of stochastic channels or in other terms the number of service antennas gets higher and higher, it is the *law of the large numbers*. In conventional massive MIMO, the UEs can rely to decode data on long-term *statistical* CSI (sCSI). As a consequence, no downlink (DL) pilots are needed to estimate the short-term *instantaneous* CSI (iCSI) [17].

Whereas in cell-free massive MIMO, the channel hardening is less accentuated owing to its distributed architecture. Practically, a specific UE is served only by a cluster of APs especially the nearest ones, because the signals transmitted by the farthest APs are degraded by large path-loss. Thus, the number of APs taking into consideration for serving the UEs is small and the law of the large numbers is not valid. So, the UEs, having low degree of channel hardening, rely on iCSI based on beamformed DL pilots [10, 14, 18]. Besides, UEs whose channels vary quickly need to use beamformed DL pilots to acquire iCSI. Hence,

the pilot utility metric per UE [14] is measured not only by the channel hardening degree but also by the speed of UEs. It is to mention that in conventional massive MIMO, only UEs whose channels vary slowly don't need to receive beamformed DL pilots. But, this is not the case for UEs whose channels vary quickly. As a consequence, the use of DL pilots will overwhelm the limited radio resource at the price of data. To this end, we should have recourse to save resources while assigning the DL pilots to the UEs. Hence, using pilot assignment strategies become relevant to mitigate the DL pilot contamination in cell-free massive MIMO.

1.2.2 Related works

A broad spectrum of methods have been applied to reduce pilot overhead and the IUI in communication systems. Among these methods, we may cite the pilot assignment, which can be formulated as a combinatorial problem, resulting in an excessive computational complexity [19]. This has boosted the design of suboptimal greedy pilot assignment algorithms, which exploit statistical information such as the large-scale fading to enhance the max-min fairness spectral efficiency and reduce UL pilot contamination between cells in massive MIMO [20].

In cell-free massive MIMO, to reduce the pilot overhead, the authors in [14] considered a pilot utility metric to decide whether a UE needs an orthogonal DL pilot beamformed by each AP to acquire the DL channel gain or just rely on statistical channel to guarantee higher DL per-user and sum throughput. However, in practice, the coherence interval length is limited. For orthogonal pilot assignment, the size of pilots is equal to the number of UEs, i.e., number of unique pilots. When the pilot gets longer, this causes more and more pilot overhead at the expense of sending data. As the number of UEs can go to infinity, the number of orthogonal sequences should be as small as possible to reduce pilot overhead. To that end, pilots are reused or non-orthogonal pilots are used. In that respect, in cell-free massive MIMO, many papers used random pilot assignment, i.e, each UE will be randomly assigned one pilot sequence from a set of orthogonal pilot sequences [8, 21]. Its strongest part is the simplicity and the susceptibility to be used in distributed networks. However, its weakest part is that it does not take into consideration the case when UEs in close vicinity use the same pilot. This leads to a severe pilot contamination in cell-free massive MIMO. To deal with this weakness in such systems, appropriate pilot assignment schemes are needed to mitigate pilot contamination and to reduce pilot overhead. Greedy

pilot assignment algorithm in [8] allows to assign randomly UL pilots to all UEs. Then, this assignment is improved iteratively by selecting the UE corresponding to the minimum per-user DL rate. The selected UE updates its UL pilot so that its pilot contamination effect is minimized. Moreover, [15] proposed a joint UL-DL pilot assignment algorithm to minimize a utility function taking into consideration the UL and DL pilot contamination ensuring uniform quality of service throughout the network. Another method to cope with reducing pilot overhead is the clustering pilot assignment. Among these schemes, a regular pilot reuse scheme is adopted in [22] to guarantee that UEs sharing a copilot are sufficiently geographically separated, and to keep pilot contamination at an acceptable low level. Moreover, to control the pilot contamination in cell-free massive MIMO, [23] proposed a dynamic cooperation clustering, which is a user-centric approach where each UE is served by the AP subset providing the best channel conditions.

In addition to that, the graph coloring algorithms, being minimization techniques, have been implemented to reduce the interference in mobile communications [24, 25]. Reference [26] proposes a pilot assignment algorithm based on vertex graph-coloring problem to model reusing UL pilots between multiple cells in cellular networks. Precisely, in [26], UL pilot contamination occurs only between cells because a pilot can be used once within one cell. The graph theoretic approach was also used to assign DL training pilots in order to reduce the pilot overhead in centralized massive MIMO systems [25]. Furthermore, it was used for UL pilot assignment in [24], by exploiting the large-scale fading coefficients in massive MIMO systems. The reference [24] studied the UL interference effect that one UE can impact on another UE when sharing the same UL pilot in massive MIMO. In such a system, DL pilots are not needed thanks to the channel reciprocity and the channel hardening. This is valid under the assumption of low/moderate speed UE. Assuming low degree of channel hardening and high-speed UEs, the study in [24] can be extended to the case of DL interference in cell-free massive MIMO.

As a consequence, the ***research question of our thesis*** is as follows:

It will be appropriate to determine under which conditions UEs can reuse the same DL pilot without causing DL pilot contamination in cell-free massive MIMO.

1.3 Contributions of the thesis

In response to the research question of our thesis, in cell-free massive MIMO, we study a reuse of pilots strategy based on a coloring graph theory. As far as we know, no previous

research has investigated the use of graph coloring for DL pilot assignment in cell-free massive MIMO to mitigate the DL pilot contamination. Hence, the innovation and novelty of this paper are orientated towards this issue. Different from [15], which dealt with the use of non-orthogonal UL and DL pilots to study the gain introduced by the DL beamforming training in cell-free massive MIMO, we used orthogonal UL pilots and non-orthogonal DL pilots to study the potential DL interference between UEs. Specifically, our contributions are laser-focused on the following points:

- We propose a metric to measure *the strength of potential IUI between two UEs*. It is a ratio of the interference channel strength and the desired channel strength, deduced from the per-user DL rate.
- We construct an *interference or a conflict graph* to describe the potential IUI relationship among all UEs in cell-free massive MIMO. UEs, between which the ratio of the interference channel strength and the desired channel strength is stronger than a certain threshold, are in conflict, i.e., are connected to each other.
- We propose a *graph coloring algorithm* to greedly assign different pilots to connected UEs and the same pilot to non-connected UEs in the conflict graph in cell-free massive MIMO.
- We study the improvement of the performance gain of the proposed graph coloring algorithm for pilot assignment in cell-free massive MIMO, compared to those based on sCSI, orthogonal pilot assignment and random pilot assignment in the DL training.
- We study the *reduction of the DL pilot overhead ratio* versus the number of UEs using the proposed scheme, comparing the other pilot assignment schemes in the DL training.

1.4 Organization of the thesis

The remaining part of this thesis revolves around 3 chapters as follows:

- ***Chapter 2***, introduces the fundamentals of massive MIMO systems, including the paradigm shift from point-to point MIMO to massive MIMO systems and its features. Added to that, we focus on the benefits and challenges while adopting massive MIMO systems;

- ***Chapter 3***, describes the reason to shift from a massive MIMO system to cell-free massive mimo. It presents the key features of cell-free massive MIMO. Besides, it describes a cell-free massive MIMO system model that we will adopt in our work. Later, we make a deep performance analysis on the achievable DL rate under statistical and instantaneous CSI. In addition to that, it presents some practical deployments and approaches in cell-free massive MIMO;
- ***Chapter 4***, is dedicated to our contribution in this thesis dealing with a graph theorethic approach for DL pilot assignment in cell-free massive MIMO. Later, we assess the improvements of our contribution compared to prior works;
- ***Chapter 5***, gives concluding remarks including a summary of our contributions. We discuss our perspectives to extend our work. The publication related to this thesis is accessible in Appendix A.

Chapter 2

Fundamentals of massive MIMO

> *You don't have to see the whole staircase, just take the first step.*
>
> *Martin Luther King Jr.*

Contents

2.1 Introduction

This chapter describes the paradigm shift from MIMO to massive MIMO while focusing on the purpose of scaling up the number of antennas especially for beamforming. On the one hand, it studies the pros and cons of the massive MIMO system. On the other hand, we study a common problem in massive MIMO systems called "pilot contamination".

2.2 On the road to massive MIMO

In MIMO systems, we can distinguish two types depending on the number of UEs receiving simultaneously the data using the same carriers: single-user MIMO (SU-MIMO), denoted also point-to-point MIMO and multi-user MIMO (MU-MIMO) [3]. SU-MIMO consists of a transmitter and receiver, equipped with more than one antenna for wireless communications. It assigns the bandwidth of a wireless access point to a single UE at a time. But, it requires complex and expensive multi-antenna UEs. Added to that, in such a system, the multiplexing gain is constrained by the minimum of the number of antennas at the receiver and the transmitter [3], this limits the achievable rate. Furthermore, in cellular networks, especially at the edge of the cell, where UEs suffer from a low SNR, the multiplexing gain may disappear [3].

With MU-MIMO, we rely on parallel transmission, where the BS is able to send and receive data from multiple UEs at a time, by exploiting the channel coefficients. As a consequence, the improvements of using MU-MIMO in cellular networks are as follows [27]:

- Increasing data rate: As with more antennas, more independent data streams can be sent out and the more UEs can be served simultaneously;
- Enhancing reliability: As the more antennas are, the more distinct paths that the radio signal can propagate over, i.e., it is a multipath propagation. This phenomenon is called "spatial diversity";
- Improving energy efficiency (measured in bits/J): because the BS can focus its emitted energy into the spatial directions towards intended UEs, reducing the energy waste due to interference leakage; and
- Reducing interference: With same transmit power, the more antennas are, the more directivity is towards an intended UE, illustrated by the main lobe, and less leakages

or interference in the other directions, illustrated by the side-lobes.

All above improvements cannot be achieved simultaneously, and there are requirements on the propagation conditions.The idea of using this type of multi-antenna technology to transmit data to many UEs has been around for a long time. It has been given different names: (i) in the DL, from the BS to the UEs, called *multi-user beamforming* or multi-user precoding; and (ii) in the UL, from different UEs to BS and it tried to separate different signals, it has been called *multi-user detection*. For example, in 1987 the first works around the idea of using many antennas to receive signals came up by Jack winters [28]. Then, there are some works from the early 90s [29,30] that were also turned this around and using multi-user beamforming to send signals in the DL. Moreover, the idea of using multiple antennas had also been around a number of different standards in particular different version of LTE in 2008 and different Wi-Fi standards as 802.11ac in 2013. The most modern standard, LTE-Advanced, allows for up to 8 antenna ports at the BS.

However, with MU-MIMO, UEs and BS compete for time to communicate on the same channel causing the co-channel interference [31]. To ensure co-channel separation between users, precoding and receive processing are achieved. Added to that, using a few number of antennas has disappointing results such as small theoretical gains. Furthermore, we still have side-lobes (interference) in a non-desired direction. Then, we get insufficiently accurate knowledge about the channel. As a result, with a limited number of anntennas, we can't point the beam in the intended direction and avoid interference at underside directions. As a consequence, the more antennas the BS/UEs is/are equipped with, the better performance is.

Then, the massive MIMO concept showed up taking the technique of multi-user MIMO idea to another level. Massive MIMO system [4] was proposed by the pioneer, Dr. Thomas Marzetta. He particulary looked at having an unlimited number of antennas at the base station in cellular networks. The idea was denied by researchers, as we can never put out an unlimited number of antennas in a finite sized dimension. However, they started to accept that maybe an infinite number of antennas is unreasonable but we only need hundreds of antennas. Hence, by convention, massive MIMO makes use of hundreds of antennas at the BS to serve tens of UEs simultaneously in the same time-frequency resource. Scaling up massively the number of antennas brings benefits compared to MU-MIMO. It will be detailed later throughout the section 2.4.

2.3 Massive MIMO systems

Massive MIMO system is a MIMO technology where the base station has many more number of antennas, M, than number of UEs, K, i.e. $M \gg K$, simultaneously served in the same time-frequency resources. Prior to presenting the massive MIMO characteristics and its processing, let's start by mathematical preliminaries as follows:

2.3.1 Mathematical preliminaries

2.3.1.1 The law of large numbers and the central limit theorem

Suppose X a random variable with a population mean μ and a variance σ^2. We consider a sample of population X, $\{X_1, X_2, \cdots, X_n\}$, composed of independent random variables with the same underlying distribution. In this case, we consider that the X_i are independent and identically-distributed (i.i.d). In particular, the all X_i terms have the same mean μ and variance σ^2.
For each n, let $\overline{S}_n$ be the sample mean, the average of the n samples of variables collected $X_1, X_2, \cdots, X_n$ as follows:

$$\overline{S}_n = \frac{X_1 + X_2 + \cdots + X_n}{n} = \frac{1}{n}\sum_{i=1}^{n} X_i \tag{2.1}$$

It is to mention that $\overline{S}_n$ is a random variable. Considering these hypothesis, we get the following law and theorem:

- ***The law of large numbers*** (to determine the value of $\overline{S}_n$ when n grows):
  As n grows, the probability that $\overline{S}_n$ is close to μ goes to 1. In other terms, when n grows, the sample mean $\overline{S}_n$ is close to population mean μ.
- ***The central limit theorem*** (to determine the distribution of $\overline{S}_n$ when n grows):
  As n grows, the distribution of $\overline{S}_n$ converges to the normal distribution $\mathcal{N}(\mu, \sigma^2/n)$.

2.3.1.2 Matrix conditioning

The linear models of telecommunications systems often lead to the resolution of large linear systems, which can be presented matricially by a linear system $A\boldsymbol{x} = \boldsymbol{b}$, where A is a matrix and $\boldsymbol{b}$ the second member. In order to control the validity of a calculated solution $\boldsymbol{x}$ compared to these data $\boldsymbol{b}$, the *conditioning* of a matrix measures the dependence of the

solution $\boldsymbol{x}$ of a numerical problem on the data of the problem $\boldsymbol{b}$. Indeed, the data of a numerical problem generally depend on experimental measurements and therefore contain errors. In other terms, if we make a small change on A, how it will affect our solution vector $\boldsymbol{b}$, i.e., we get a small or a large change on $\boldsymbol{b}$, and vice versa.
The conditioning of a matrix A is measured via a condition number of a matrix A, defined as follows:

$$\text{Cond}(A) = \|A\|\|A^{-1}\| \geqslant \|AA^{-1}\|, \text{where } \|.\| \text{ is a matrix norm.} \tag{2.2}$$

It is to notice for whatever matrix norm, the norm of identity matrix I is equal to 1.
As $I = AA^{-1}$ and $\|A\|\|A^{-1}\| \geqslant \|AA^{-1}\|$, then $\text{Cond}(A) \geqslant 1$. $\text{Cond}(A)$ is an indicator to reveal if the system to be studied is ill-conditioned or well-conditioned. The different possible cases of the value $\text{Cond}(A)$ are as follows:

- If $\text{Cond}(A)$ is near to 1, then the matrix A of the problem is *well-conditioned*, i.e. a **small** variation on $\boldsymbol{b}$ leads to a **small** variation on $\boldsymbol{x}$.
- If $\text{Cond}(A)$ is very large compared to 1, then the matrix A of the problem is badly or *ill-conditioned*, i.e. a **small** variation on $\boldsymbol{b}$ leads to a **large** variation on $\boldsymbol{x}$. Measuring devices are never perfect, and it is impossible to know exactly $\boldsymbol{b}$. This can cause very great inaccuracy in the value of $\boldsymbol{x}$.

2.3.2 Massive MIMO Processing

2.3.2.1 Two configurations of TDD frame

As M goes large in massive MIMO system, TDD operation is appreciated (see later in paragraph 2.3.3.1). As in [5], two configurations of a TDD frame are available, differing only in including or not DL pilots. The guard time intervals between UL and DL transmissions are not shown. The first configuration, shown in Figure 2.1(a), includes UL training, UL data DL training and DL payload data transmission. These phases will be described in details in the following paragraph. Compared to the first configuration, the second one, shown in Figure 2.1(b), doesn't include DL pilots. We denote $\tau_c = T_c B_c$ the length of coherence interval, where T_c is the coherence time and B_c is the coherence bandwidth. Moreover, τ_c can be written as the sum of the length of every subinterval as follows

$$\tau_c = \tau_{ul,d} + \tau_{ul,p} + \tau_{dl,p} + \tau_{dl,d}, \tag{2.3}$$

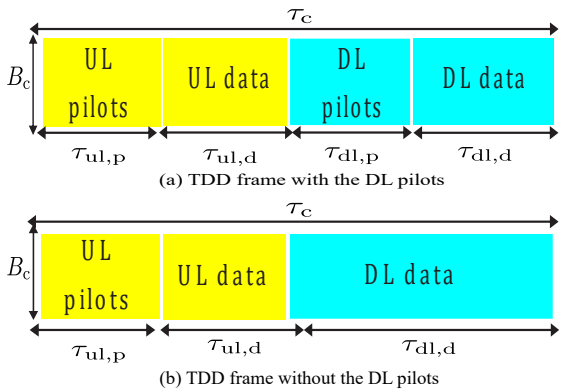

(a) TDD frame with the DL pilots

(b) TDD frame without the DL pilots

Figure 2.1: The TDD frame containing $\tau_c = T_c B_c$ symbols, where T_c and B_c are, respectively, the coherence time and the coherence bandwidth.

where $\tau_{\text{ul,d}}$ and $\tau_{\text{ul,p}}$ are, respectively, the number of symbols per TDD frame used in the UL to send data and pilots. $\tau_{\text{dl,d}}$ and $\tau_{\text{dl,p}}$ are, respectively, the number of symbols per TDD frame used in the DL to send data and pilots.

The TDD frame structure is generally designed to be smaller or equal to the smallest channel coherence interval of all active UEs. For the sake of simplicity, throughout the report, we assume that a TDD frame is equal to the channel coherence interval. Added to that, the coherence interval is split into UL and DL subintervals.

2.3.2.2 UL and DL channels in TDD frame

As it is mentioned in [3, 32], in TDD system, the UL and DL channels use the same frequency spectrum, but different time slots. We suppose that the UL and DL channels are reciprocal thanks to an accurate hardware chaine calibration. We notice that the precoding requires a high quality of CSI at the transmitter. The CSI can be obtained differently depending on UL/DL communications:

- In the UL channel, precisely, in the UL training phase (UL pilots), the UEs send known signals, called pilots, to the BS. Subsequently, the latter estimates the UL CSI from all UEs, based on the received pilot signals. Thanks to the channel reciprocity, this CSI is used to precode the transmit signals in the DL (DL data) and to detect the signals sent from the UEs in the UL (UL data). The sine qua none conditions of this process is that K channels are occupied.
- In the DL channel, the DL CSI is needed by the BS and may be needed by the UE,

depending on the channel hardening and the speed of UE [14]; (i) On the BS side, the DL CSI is needed to precode the transmitted signals. Thanks to reciprocity, the channel estimated in the UL is used to precode the transmitted data; (ii) On the UE side, the effective DL channel gain is used to decode the desired signals. To obtain the DL channel information, the BS can beamform pilots (DL pilots). Relying on the received signal, each UE can estimate the effective DL channel gain. The sine qua none conditions of this process is that K channels are occupied.

As a consequence, the channel estimation process needs a minimum of $2K$ channel uses. If we assume that the channel is constant over T symbols. Thus, we have $2K < T$. It is to mention that TDD frame phases are interchangeable. The activities within the frame are not rigorously sequential as long as we do not alternate the UL and the DL [5,32]. It is however important to switch to DL data transmission (resp. UL data transmission), quickly after the UL training so that the precoding (resp. detection) is based on good UL channel estimates.

2.3.3 System Characteristics

2.3.3.1 TDD operation is prefered in massive MIMO

TDD operation is recommended in massive MIMO system, as M is large, because the training overhead is independent of the number of BS antennas, unlike FDD operation [5, 32]. To go deeper, in FDD systems, the number of BS antennas and the number of UEs are limited by $M + K < T$. In contrast, in TDD systems, the limitation on M and K is $2K < T$ as it is demonstrated above. To illustrate the reason that massive MIMO prefers TDD operations, we assume a coherence interval with T = 200 symbols (with a coherence bandwidth of 200 kHz and a coherence time of 1 ms). Then, in FDD systems, the number of BS antennas and the number of UEs are constrained by $M + K < 200$, while in TDD systems, the constraint on M and K is $2K < 200$. Figure 2.2 shows the region of possible values (M, K) in FDD and TDD systems. As it is shown the TDD region is bigger than the FDD region. As a consequence, adding more antennas is impartial of the channel estimation overhead. We assume half-duplex TDD so that only one end of the link is transmitting at any one time, either the BS or the UEs. The channel coherence interval describes the time-frequency interval during which the channel response can be considered almost constant. It is determined by the propagation environment, UE mobility, and carrier frequency [5].

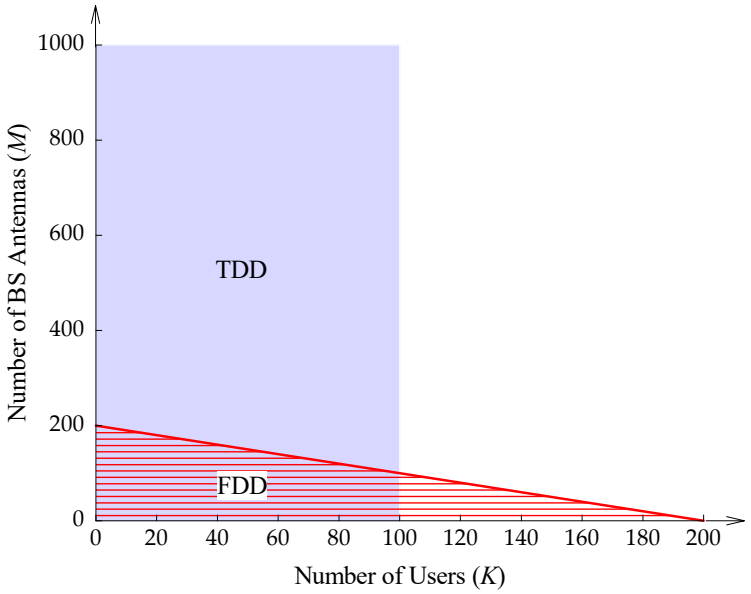

Figure 2.2: The possible values of (M, K) in TDD and FDD systems, for a coherence interval of 200 symbols.

2.3.3.2 Massive MIMO provides a favorable propagation

Favorable propagation means a mutual orthogonality amongst the vector-valued channels to the UEs. In other terms, the channel matrix between the BS antenna array and the UEs is well-conditioned (see Section 2.3.1.2). In massive MIMO, under some conditions, the favorable propagation property holds thanks to the law of large numbers, i.e., the channel vectors between the base station and the UEs are pairwisely (nearly) orthogonal [33]. In other terms, the propagation channel responses from the BS to different UEs are sufficiently different (i.e., their inner products are zero).

2.3.3.3 Simple linear processing

To obtain optimal performance, complex signal processing techniques must be implemented. The BS can use linear processing schemes (linear receivers in the UL and linear precoders in the DL) to reduce the signal processing complexity. However, these schemes are not optimal. As the number of BS antennas and of UEs are tremendous, the signal processing at the UE side must rely on large dimensional matrices. As a consequence, simple signal processing is recommended to reduce system complexity. In massive MIMO, the channels are favorable thanks to the law of large numbers. As a consequence, linear processing (lin-

ear detecting schemes in the UL and linear precoding schemes in the DL) is nearly optimal as it is revealed in [3, 4] (see example of detectors in section 2.4).

2.3.3.4 Scalability

The scalability of massive MIMO is revealed by the following points:

- **Channel estimation**: In massive MIMO, the BS estimates the channels via UL training, under TDD operation. The time required for channel estimation doesn't depend on the number of BS antennas. Then, we can scale up the number of BS antennas without affecting on the channel estimation overhead.
- **Signal processing**: The signal processing at each UE is very simple and does not depend on other UEs' existence, i.e., no multiplexing or de-multiplexing signal processing is performed at the UEs. Making one UE active or not is independent of other UEs activities. To illustrate this, see example in section 2.4.

2.3.3.5 Channel hardening characteristic in massive MIMO

Channel hardening is a channel feature where the norms of the channel vectors between the BS and the k-th UE defined by $h_k,\ k = 1 \cdots K$ fluctuate only little. When the number of BS antennas is large, the channel becomes (nearly) deterministic, and hence, the effect of small-scale fading is averaged out as follows

$$\frac{\|\mathbf{h}_k\|^2}{\mathbb{E}\left\{\|\mathbf{h}_k\|^2\right\}} \to 1 \text{ as } M \to \infty, \text{i.e. } \|\mathbf{h}_k\|^2 \sim \mathbb{E}\left\{\|\mathbf{h}_k\|^2\right\}.$$

Therefore, massive MIMO is characterized by a high channel hardening, as a consequence of the law of large numbers. To measure the channel hardening, we calculate the variance of $\frac{\|\mathbf{h}_k\|^2}{\mathbb{E}\left\{\|\mathbf{h}_k\|^2\right\}}$, defined as $\mathbb{V}\left\{\frac{\|\mathbf{h}_k\|^2}{\mathbb{E}\left\{\|\mathbf{h}_k\|^2\right\}}\right\}$ (see eq 2.17 in [2]),

- If $\mathbb{V}\left\{\frac{\|\mathbf{h}_k\|^2}{\mathbb{E}\left\{\|\mathbf{h}_k\|^2\right\}}\right\} \to 0$ as $M \to \infty$, we have a high channel hardening.

To understand the effect of increasing the number of antennas on the channel hardening, let's try to link the channel hardening with spatial diversity. The small-scale fading is a random fluctuation in the channel gain, caused by microscopic changes in the propagation environment. These random fluctuations make the channel unreliable. To combat this

problem, we have recourse to spatial diversity, sending the signal over multiple channels with independent realization. Let's try to understand how the spatial diversity increases the reliability of the channel in the following example. We assume that the probability of a bad channel gain is $p = 0.1$. Then, depending on the number of antennas at the base station, we get different channel reliability.

- With a BS with single antenna, there is $p * 100\% = 10\%$ of risk of getting a bad channel.
- With a BS with $M = 8$ antennas, if we have M antennas with independant channel gain, the overall risk that they are bad is equal to $p^M = \underbrace{p \times p \times \cdots \times p}_{M \text{times}}$, there is $p^M * 100\% = 0.00001\%$ of risk of getting a bad channel.

We conclude that the more the BS is equipped with antennas, the more the channel hardens.

2.3.3.6 Constraints on massive MIMO antenna array size

The size of the BS antenna array in massive MIMO systems must not be large as the distance between two antennas is evaluated to half a wavelength. For instance, as depicted in Figure 2.3, 128-antenna cylindrical array is composed of 4 circles, where each of it is composed of 16 dual-polarized antenna elements. At 2.6 GHz, the distance between two adjacent antenna elements is about 6 cm, which is equal to 1/2 a wavelength. Hence, the physical size of such a system is 28cm×29cm [34].

Figure 2.3: Cylindrical patch array

2.4 Massive MIMO benefits

Opting for a massive MIMO system has the following specific benefits:

- **Simple signal processing**: Using an immoderate BS antennas compared to the number of active UEs yields the performance of simple linear processing nearly optimal. More precisely, even with simple maximum-ratio combining (MRC) in the UL or maximum-ratio transmission (MRT) in the DL, the effects of fast fading, intracell interference, and uncorrelated noise tend to disappear as the number of BS station antennas grows large. To explain this point, we consider the following example:
  Example: Using maximum-ratio combining (MRC) in the UL transmission with i.i.d. Rayleigh fading channel

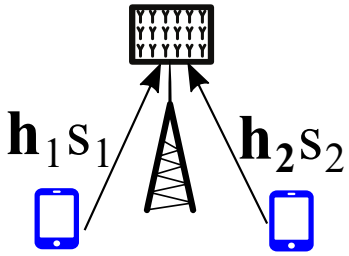

Figure 2.4: A basic massive MIMO system to demonstrate the effect of using MRC.

As it is shown in Figure 2.4, the system features are as follows:

- 2 UEs send signals s_k for $k = 1, 2$
- Channels $\mathbf{h}_k = [h_{k1} \cdots h_{kM}]^T \sim \mathcal{CN}(0, \mathbf{I}_M)$
- Noise: $\mathbf{n} \sim \mathcal{CN}(0, \mathbf{I}_M)$
- The signal received at the BS: $\mathbf{y} = \mathbf{h}_1 s_1 + \mathbf{h}_2 s_2 + \mathbf{n}$
- The signal detected by UE_1, $\tilde{y}_1$, using a linear detector MRC for UE 1, whose expression $\mathbf{v}_1$ is as follows $\mathbf{v}_1 = \frac{1}{M}\mathbf{h}_1$:

$$\tilde{y}_1 = \mathbf{v}_1^{\mathrm{H}}\mathbf{y} = \underbrace{\mathbf{v}_1^{\mathrm{H}}\mathbf{h}_1 s_1}_{\text{desired signal}} + \underbrace{\mathbf{v}_1^{\mathrm{H}}\mathbf{h}_2 s_2}_{\text{interference signal}} + \underbrace{\mathbf{v}_1^{\mathrm{H}}\mathbf{n}}_{\text{noise signal}}$$

Thanks to the law of large numbers, we have
$\mathbf{v}_1^{\mathrm{H}}\mathbf{h}_1 = \frac{1}{M}\|\mathbf{h}_1\|^2 \xrightarrow[M\to\infty]{} \mathbb{E}\{|h_{11}|^2\} = 1$, i.e., the desired signal remains;
$\mathbf{v}_1^{\mathrm{H}}\mathbf{h}_2 = \frac{1}{M}\mathbf{h}_1^{\mathrm{H}}\mathbf{h}_2 \xrightarrow[M\to\infty]{} \mathbb{E}\{h_{11}^{\mathrm{H}} h_{21}\} = 0$, i.e., the interference signal vanishes;
$\mathbf{v}_1^{\mathrm{H}}\mathbf{n} = \frac{1}{M}\mathbf{h}_1^{\mathrm{H}}\mathbf{n} \xrightarrow[M\to\infty]{} \mathbb{E}\{h_{11}^{\mathrm{H}} n_1\} = 0$, i.e., the noise signal vanishes.

As a consequence, we have $\tilde{y}_1 \xrightarrow[M\to\infty]{} s_1$. As M goes large, it is an asymptotically noise and interference-free communication.

- **Massive MIMO can enhance the *spectral efficiency* by a factor of 10 or more and at the same time, boost the radiated *energy efficiency by 100***:
  The explanation of these benefits is structured around 3 points and illustrated by an example as follows:

  (i) *Enhancing the spectral efficiency*: The capacity increase results from the big spatial multiplexing gain used in massive MIMO. As a consequence, the spectral efficiency is enhanced and it grows proportionally with the number of UEs. For instance, when we have 10 active UEs, that means we can get roughly 10 times higher spectral efficiency than in a system with only one UE.

  (ii) *Enhancing the energy efficiency*: Massive MIMO enhances the radiated energy efficiency compared to conventional MU-MIMO; The directivity with a big number of antennas at the base station is much stronger than with few antennas. So, we get very directive signals, laser-focused towards the intended UE and less interference leakage, i.e. energy can be concentrated with extreme sharpness into tiny areas (see Figure 2.5 [3,31]). By appropriately beamforming the signals sent out by the antennas, the BS can ensure that the beams emitted by its whole antenna array sum up constructively towards the intended UE, but destructively (randomly) almost everywhere else. The interference between UEs can be suppressed more and more using, e.g., zero-forcing (ZF). But, this can come at the expense of further transmitted power, as depicted in Figure 2.5. Added to that, laser-focusing the signal towards the intended UE, via increasing the antennas BS, can potentially boost the power efficiency. The transmitted power is reduced in the UL for the UEs, draining their battery slower, and the emitted RF power is decreased for the BS in the DL, reducing the electricity consumption at the BS [35].

  (iii) *Tradeoff between energy efficiency and the spectral efficiency*: This is illustrated quantitatively in Figure 2.6 [31]. Precisely, it presents the tradeoff between the *energy efficiency* as the entire number of bits (sum-rate) transmitted per Joule per

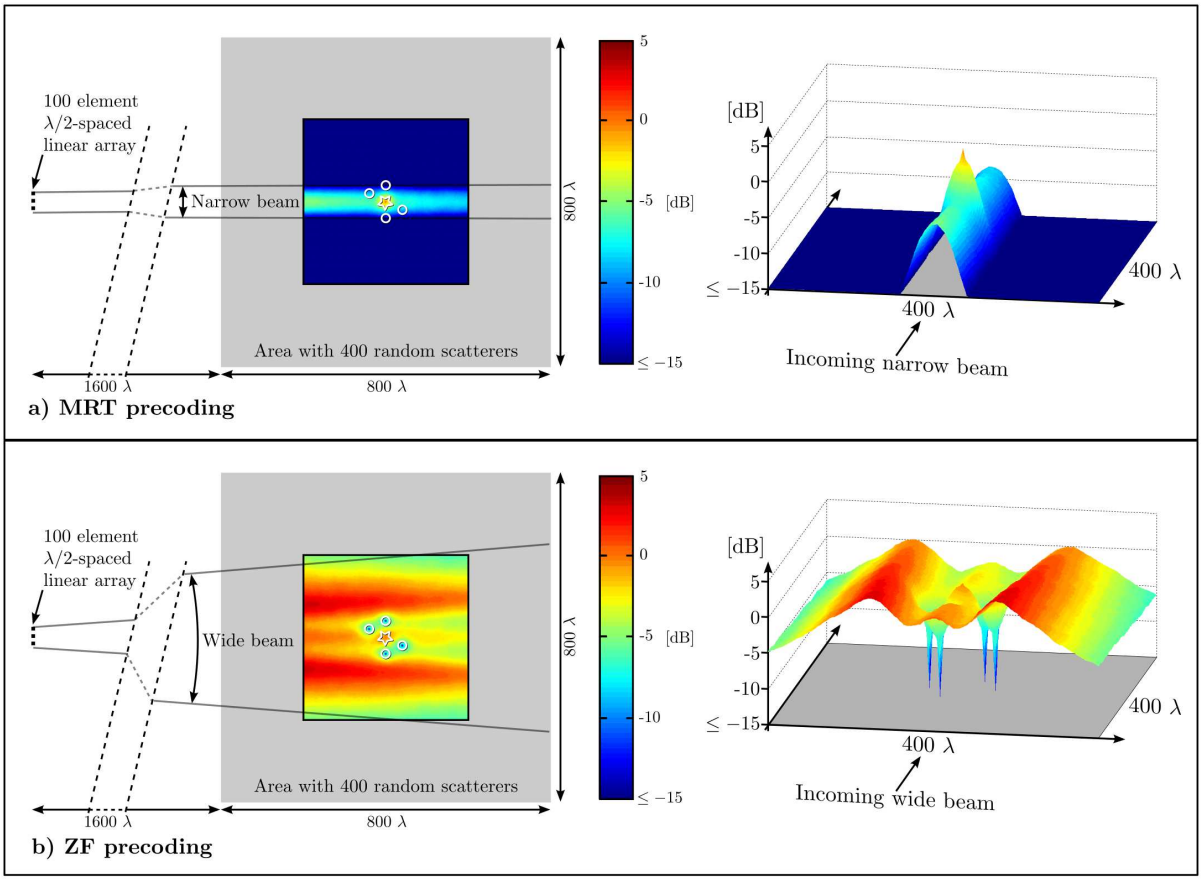

Figure 2.5: Relative field strength around a target UE in a $800\lambda \times 800\lambda$-sized scattering environment, when the BS is placed 1600λ to the left. Average field strengths are calculated over 10000 random placements of 400 scatterers, when 2 different linear precoders are used: a) MRT precoder and b) ZF precoder. Left: pseudo-color plots of average field strengths, with target UE positions at the center (symbolized by a star), and 4 other UEs nearby (symbolized by 4 circles). Right: average field strengths as surface plots, allowing an alternative view of the spatial focusing.

UE receiving service of energy spent, and *spectral efficiency* defined by the entire number of bits (sum-rate) transmitted per unit of radio spectrum consumed. It depicts the relation for the UL, from the UEs to the BS.

The Figure 2.6 depicts the tradeoff for 3 cases:

1) The first case (purple), a benchmark system with a single-antenna BS serving one UE;

2) The second system (green), a system with 100-antenna BS serving a single

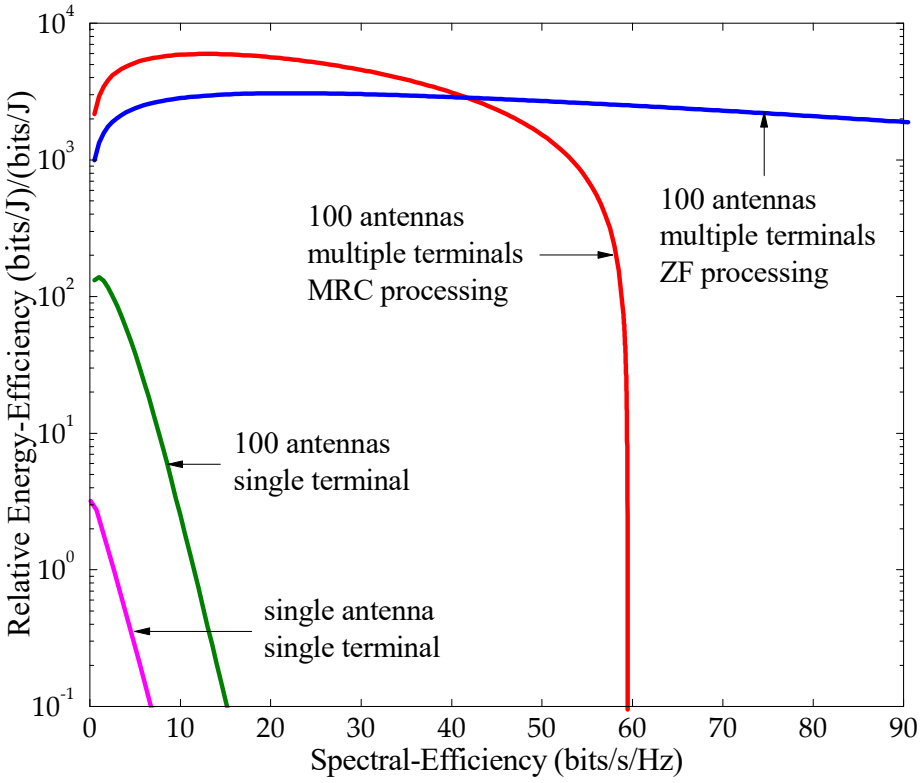

Figure 2.6: Improving UL spectral efficiency 10 times and simultaneously increasing the radiated-power efficiency 100 times with massive MIMO technology, using extremely simple signal processing.

UE using conventional beamforming;

3) The third system (red, using MRC; and blue, using ZF), a massive MIMO system equipped with 100-antenna BS simultaneously serving multiple (about 40 here) UEs.

The attractiveness of MRC compared to ZF is not only its computational simplicity, i.e., as its process of decoding consists in projecting the received signals onto the conjugate channel responses, but it can also be used in a distributed manner, independently at each antenna unit. While ZF is efficient for a conventional MIMO system as well as MIMO system with few number of antennas, MRC generally is not. What makes MRC work perfectly for massive MIMO is that the channel responses between the UEs and the BS antennas are almost

orthogonal when the antenna number goes high [36].

The prediction in Figure 2.6 relies an information-theoretic analysis combining the intra-cell interference, the bandwidth and energy cost of using pilots to estimate the CSI when it comes to high-mobility environment [31]. Considering the MRC receiver, it performs in the nearly noise-limited regime of information theory. In other terms, each UE is provided with about (1 b/s/Hz). In a massive system, while using MRC ("green" regime), we decrease the power as without serious repercussions on the overall spectral efficiency, multiuser interference and effects from hardware imperfections are overwhelmed by the thermal noise.
The overall spectral efficiency, which is 10 times higher than in conventional MIMO system, is brought about serving many tens of UEs simultaneously, in the same time-frequency resource. When we operate in the 1 bit/dimension/UE regime, the inter-symbol interference can be regarded as additional thermal noise [37]. As a consequence, this offers a path to dispose with orthogonal frequency-division multiplexing (OFDM) to combat the inter-symbol interference. To investigate the scale of the additional capacity gains provided by massive MIMO system, we deal with an example from [31] consisting in an omni-directional 6400-antenna array ($6400 \times (\lambda/2)^2 \approx 40m^2$). It transmits with a total power equal to 120Watts(20 mW of radiating power per antenna) over a 20 MHz bandwidth in 1900 MHz. The coverage area is a disk of radius 6 km, centred by the array, which serves 1000 UEs randomly distributed inside that area. The height of the UEs and the antenna array is, respectively, 5 m and 30m. Based on the Hata-COST231 model, the path loss is equal to 127 dB at 1 km of range and a loss exponent equal to 3.52. Added to that, it is to mention that the shadow-fading follows a log-normal distribution with a standard deviation equal to 8 dB. The noise figure is equal to 9 dB. It is supposed that the channel is constant over 164 ms in order for the channel gains to be estimated with sufficient accuracy. DL data are transmitted via MRT in combination with using power control, where the 5% of the UEs, with the worst channel quality are not allowed to be served. We employ optimal max-min power control to obtain equal throughput for each of 950 UEs. Numerical averaging reveals that 95% of the UEs will receive a throughput of 21.2 Mb/s/UE. In all, this system offers to the 1000 UEs a sum DL spectral efficiency of 1000 bits/s/Hz. The max-min power

control confers an equal service at the same time to 950 UEs.

- **Massive MIMO boosts the robustness to unintended man-made interference and to intentional jamming:**
  As shown in Figure 2.7 [38], *intentional jamming* of civilian wireless networks is a growing and a serious cyber-security issue not commonly known. 100-dollar jammers and military-grade equipment can be combined together via radio-based platforms, which cost a few 1000 dollars. Myriad of incidents, precisely in public safety applications, focused on the gravity of the problem. For instance, during the EU conference, in Sweden, in 2001, demonstrators utilized a jammar located in close vicinity. During riots phases, the presence of this jammer was the trigger to not attain anyone of the police officers [38]. As the bandwidth is scarce, conveying data over frequency is unfeasible. The way to circumvent having a robust wireless communication system is to rely on pilots for channel estimation so that using smart jammers could give rise to interference via modest transmitted power. But, injecting additional smart implementation in the channel estimation and the decoding process is likely to decrease that issue.

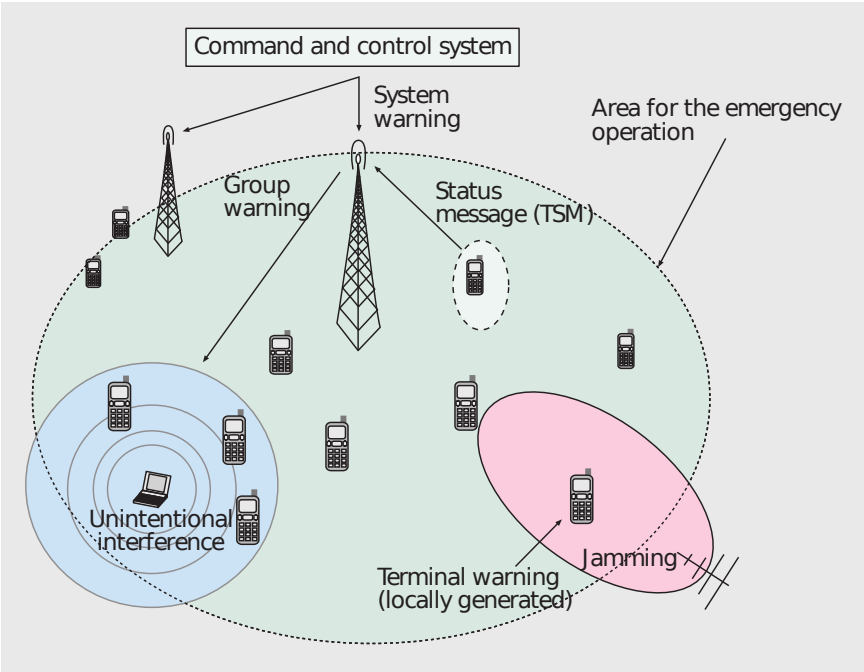

Figure 2.7: Jamming in telecommunications system.

- **Massive MIMO can be implemented with modest, low-power components:**
  The degrees of freedom of the massive MIMO system are in tremendous surplus. For instance, in case of using 200-antenna BS which serve 20 UEs, we have 200-20=180 degrees of freedom. This can be exploited to shape signals via modest hardware. Precisely, each antenna element can emit signals characterized by a tiny or constant peak-to-average ratio with a decreased total radiated power. Such (near-constant) envelope signaling makes easy the use of extremely cheap and power-efficient RF amplifiers [31].
- **Massive MIMO as a way to diminish the latency:**
  The performance of wireless communications systems is harmed by fading. The fading can decay the received signal power. It is due to the destructive interference of signals travelling from a BS to UE, from numerous paths. This phenomenon triggers low-latency wireless. The situation is more and more harmed for unlucky UEs, located in a fading dip. These UEs have to wait for the variation of the channel in order to obtain its intended data. To circumvent this issue, massive MIMO is based on beamforming via numerous antennas in line with the law of large numbers.

2.5 Massive MIMO challenges

2.5.1 Channel unreciprocity

Prior to introducing the utility of reciprocity calibration, we present a preliminary about beamforming using massive MIMO antennas, illustrated in Figure 2.8(a). Its principle is, in case numerous antennas are employed at the BS, in the DL, their respective transmit signals are likely to be aligned then they sum up constructively at the intended UE. In the UL, likewise, receive beamforming concerns the process where the numerous receive signals are well aligned and added up at the BS.

In practice, signals are altered by both magnitude and phase distortions, while going through radio frequency (RF) circuits and amplifiers; these overall RF paths magnitude and phase features undergo mismatch as depicted in Figure 2.8(b). It underlines that each antenna RF path has a specific phase and magnitude, which vary in time owing to the thermal drifts occurring in electronic components. Consequently, the numerous transmit signals sum up constructively or destructively so that they are not aligned at the intended UE. In this case, we don't notice any beamforming gain.

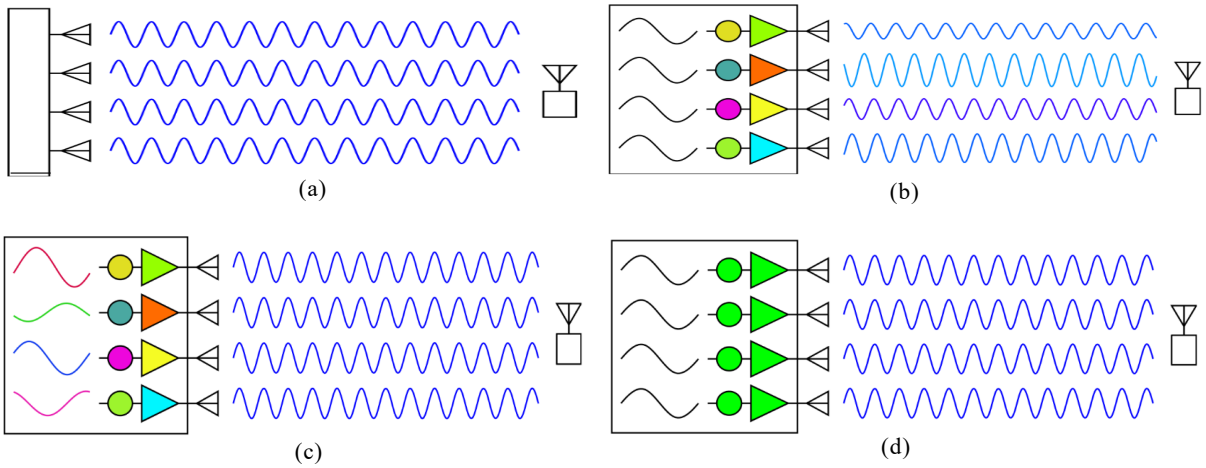

Figure 2.8: (a) Beamforming: multiple transmit signals aligned to combine constructively at the UE; (b) Mismatched wireless signals due to uncalibrated RF hardware; (c) Precoded baseband digital signals to compensate for uncalibrated RF hardware; (d) RF coherent antenna array.

In case of operating in TDD mode, the UE sends a pilot signal in the UL, and the BS estimates the channel to each antenna. Based on channel reciprocity (i.e., a matching occurs between the UL and DL), the resulted channel estimates is used in the DL channel. By common consent, the propagation channel is characterized by its reciprocity. But it can be altered by the hardware chains in the BS and the UE transceivers, resulting in non reciprocity between the UL and DL. The way to make the propagation channel be reciprocal is to have recourse to calibration of the hardware chains as it was experienced in [39,40]. In particular, [39] investigates the reciprocity calibration for a BS with 64 antennas and obtains a promoting experimental implementation.

We notice that the calibration of UL and DL chains must not be carried out to get full beamforming gains in a massive MIMO system: in case of a well calibration of the BS, the overall antenna system will emit a coherent beam to the UE. There will remain some mismatch within the UE as it is shown in Figure 2.8(b), generating non-coherent beams. The correction of RF hardware mismatch is included in the channel estimation process, it can be handled by transmitting pilots via the beam to the UE. This is denoted as *channel-estimation-based beamforming* as it is shown in Figure 2.8(c); the overhead for these pilots is very small. We notice although the baseband signals are likely synchronized, the synchronization at RF presents some challenges, as a small translation in time may cause considerable phase errors

at GHz frequencies. Then, such an approach cannot provide an accurate synchronization at the RF.

Figure 2.8(d) depicts another way to realize beamforming based on RF calibration and synchronization approaches in the antenna array, resulting in a matching in the magnitude and phase features of the whole RF paths. The antenna units are placed close to each other (separated by half-wavelength). As a result, the antenna array may perform as a phased array. In such an array, via an appropriate adjustment of the phases and magnitudes of the antenna elements, the radiation energy at specific directions can be fully focused (or removed). As depicted in Figure 2.8(d), in case the antenna units magnitudes and phases are all matched (referred to as having an RF coherent front-end), the antenna array concentrates the RF waves to combine constructively at the antenna boresight in a LoS environment.
To shift the concentration of the RF energy to another direction, to steer the beam, the magnitudes and phases (i.e., the beamforming coefficients) of each antenna can be adjusted accordingly. For instance, Figure 2.9 depicts the RF energy pattern of an 8-antenna linear array with its principal beam steered to 30°. As a consequence, in case of having RF coherent- antenna elements, the relative strength of RF energy at different angles is fixed by the beamforming coefficients.

Calibration inside the array can be forgone. As an alternative, as it was revealed in [39], one of the antennas may be regarded as a reference. Besides, to determine a compensation factor for each antenna, the signals can be traded between the reference antenna and each of the remaining antennas. Added to that,it is likely to avoid reciprocity calibration inside the array system in case of having the maximum phase difference between the UL and DL chains less than 60 degrees. Consequently, the *coherent beamforming*, as depicted in Figure 2.8(d), would be achieved with a potential 3dB reduction in gain.

2.5.2 Orthogonality of channel responses

The channel response between a UE and the BS can be described by an M-sized vector. As in general we have non-mutual orthogonality of the K channel vectors, complex signal processing such as dirty paper coding are required to prevent the interference and achieve the sum capacity of the multi-user channel. Favorable propagation channels are ideal for multi-user transmission as the inter-user interference is suppressed by simple linear processing such as MR and ZF that use the channel orthogonality property. In particular, massive MIMO (especially with MRC/MRT processing) is based on the favorable propaga-

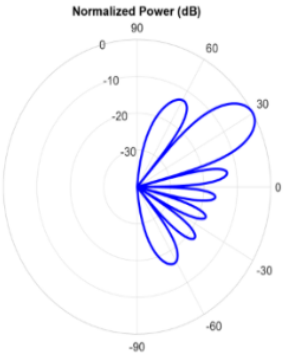

Figure 2.9: Phased array beam pattern.

tion. The question is if there exist any favorable channels in practice? The features of massive MIMO systems, the channel measurements must be carried out via realistic antenna arrays. The channel propagation responses in massive MIMO system differ from conventional smaller arrays.

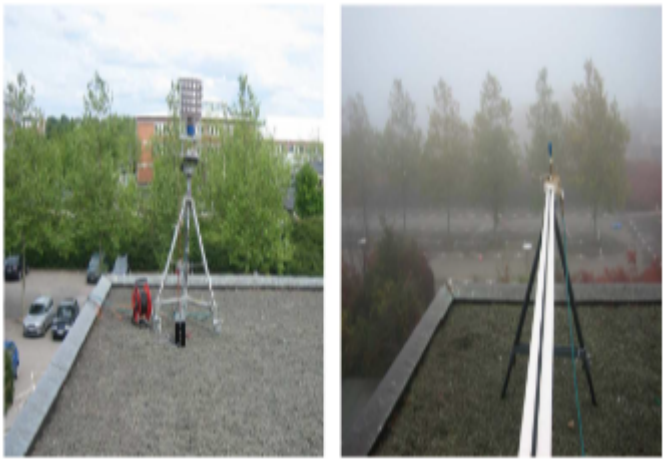

Figure 2.10: Massive MIMO array used for the mesurements.

Figure 2.10 [31] illustrates pictures of the two massive MIMO arrays carried out for the measurements. On the left, it is a compact circular massive MIMO system array with 128 antennas. It consists of 16 dual-polarized patch antenna elements organized in a circle, with 4 such circles stacked on top of each other. Added to that, being compact, it resolves likely scatterers at different heights, however its resolution in azimuth is characterized by bad performance owing to its limited aperture. On the right, there is a picture of large linear

(virtual) array, in which we turn a single omnidirectional antenna into 128-antenna array in a static environment to emulate a real array with the same dimensions [31].

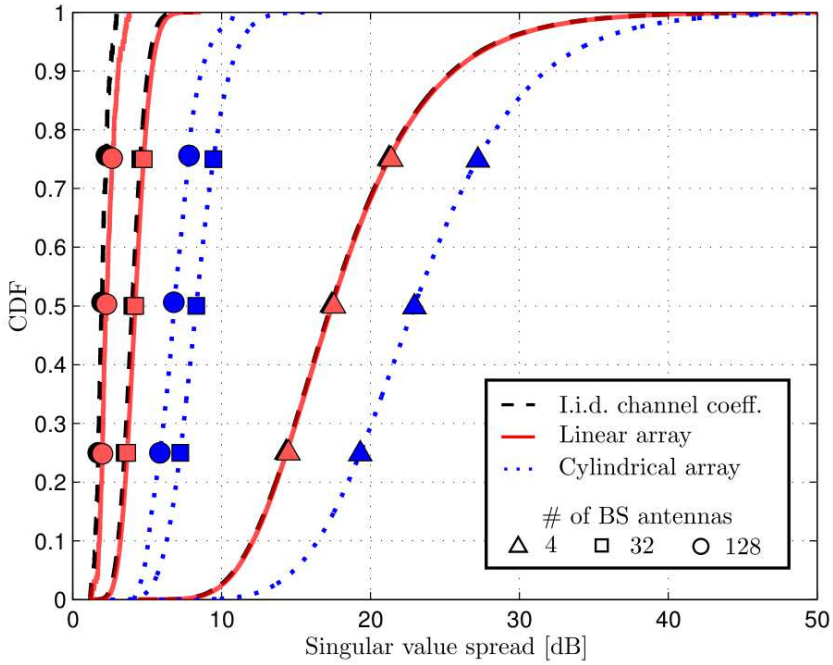

Figure 2.11: The CDF of the singular value difference for MIMO systems with 4 UEs and with 3 various numbers of antennas at the BS: 4, 32, and 128. The i.i.d. channel is regarded as a benchmark, while the other cases represent channels associated with linear and cylindrical array pattern at the BS.

To determine how much the channel responses to different UEs are, we focus on the difference between the smallest and largest singular values of the channel responses matrix. Figure 2.11 depicts this for a system with 4 UEs and a BS with, respectively, 4, 32 and 128 antennas, configured to be large single-polarized linear or compact dual-polarized circular arrays. In particular, that figure depicts the cumulative density function (CDF) of the difference between the smallest and the largest singular value in differents cases. Besides, the ideal i.i.d. channel is also shown.

All these measures were conducted in the outdoors of the Lund University campus. For that case, the center frequency was 2.6 GHz and the measurement bandwidth 50 MHz. When it comes to the cylindrical array case, RUSK Lund channel sounder was employed, while a network analyzer was employed for the synthetic linear array measures. The preliminary results of these measures were shown in [41].

For the 4-antenna array, the median of the singular value difference is, respectively, nealy 23 dB and 18 dB. This number measures the margin of fading, to serve the UEs with an acceptable received signal power. Considering the massive linear antennas system, the difference noticed is nearly less than 3 dB. Besides, the curves don't present any tail. It explains that the probability of having a singular value difference larger than 3 dB is essentially negligible.

An approximated form of favorable propagation is realized in non-line-of-sight (non-LoS) environments characterized by rich scattering, where each channel vector has i.i.d distribution with zero mean. Under these conditions, the inner products (normalized by M) go to zero (the channel vectors get closer and closer to orthogonal) as more antennas are added (as M goes large). The sine qua non condition above is applied for Rayleigh fading channels, which are commonly considered in research works on Massive MIMO, however approximate favorable propagation can be realized in many other cases as well.

Example (from [42]): Assume the BS uses a uniform linear array with $\frac{1}{2}$-wavelength antenna spacing. We compare two extreme opposite environments in Figure 2.12: (i) non-LoS isotropic scattering (i.i.d. Rayleigh fading) and (ii) LoS propagation. In LoS situation, the angle to each UE determines the channel and this angle is uniformly distributed. The simulation setup considers $M = 100$ antennas, $K = 12$ UEs, perfect CSI, and a UL SNR of $\text{SNR}_{ul} = -5$ dB. The figure 2.12 depicts the CDF of the probability of reaching a certain sum capacity, and the dashed vertical lines describe the sum capacity achieved under favorable propagation.

The isotropic scattering case yields a sum capacity near to the favorable propagation upper bound. The sum capacity in the LoS case is assimilated to that of isotropic scattering in most of cases, but there is a 10 % risk that the LoS performance loss is more than 10 %. It is due to that there is substantial probability that two UEs have similar angles [33]. An alternative solution is to prevent the few "unluckiest" UEs from service in each coherence block. Figure 2.12 depicts this by preventing 2 out of the 12 UEs. Herein, LoS propagation provides similar performance as isotropic fading.

Since isotropic and LoS propagation define 2 "extreme" environments and both are favorable in massive MIMO, we expect that real propagation environments, being between these extremes, would also be favorable. These observations explain the favorable propagation features of massive MIMO channels commonly used in measurement campaigns (e.g.,

in [43]).

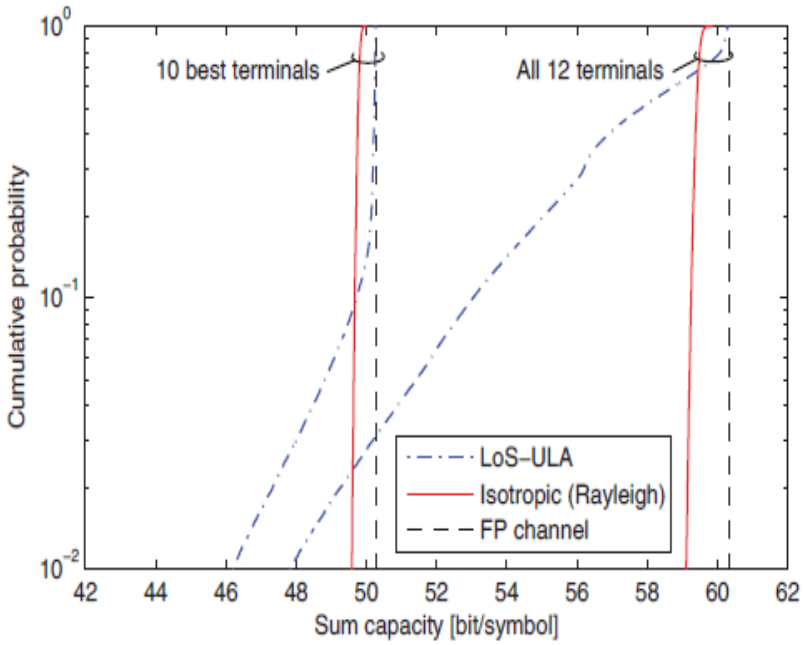

Figure 2.12: Comparison of system behavior with i.i.d. Rayleigh fading respectively LoS propagation. There are $K = 12$ UEs and $\text{SNR}_{\text{ul}} = -5$ dB. (a) CDF of the UL sum capacity with $M = 10$ antennas, serving either all 12 UEs or only the 10 best UEs.

2.5.3 Pilot reuse and pilot contamination

Whether in UL or DL, the channel information quality in conventional massive MIMO may be assigned by a pilot contamination problem [44]. It occurs during the UL/DL channel estimation, when two or more UEs send/receive non-orthogonal pilots or more precisely, the same pilot sequences. Moreover, this problem persists even when the number of BS antennas grows without bound [4,32]. As it is well explained in [2,45] intuitively to avoid this problem in UL (or DL), each UE should be assigned an orthogonal pilot in UL (or DL) to not contaminate the channel estimates in UL (or DL). However, mathematically the length of orthogonal pilot sequences is proportional to the number of orthogonal pilots, i.e., the number of UEs. Moreover, the channel coherence interval length is limited due to the changing of the propagation environment. Hence, this limits the length of orthogonal pilot sequences. Assigning orthogonal pilots cannot be physically realistic. In addition, to decode its intended data, the UE may need to rely on beamforming DL pilots. If the latters are non-orthogonal,

this will cause DL pilot contamination.

2.6 Conclusion

Relying on massive MIMO is fruitful in increasing the spectral efficiency, the capacity and the coverage by an adaptive beamforming, especially for UEs which are hard to reach with a good signal and in making the signal processing simple thanks to the favorable propagation. More precisely, even with a simple maximum-ratio combining (MRC) in the UL or maximum-ratio transmission (MRT) in the DL, the effects of fast fading, intracell interference, and uncorrelated noise tend to disappear as the number of BS station antennas grows large. Added to that, using massive MIMO enhances the energy efficiency by laser-focusing a beam towards the intended UE with less interference leakage. Furthermore, massive MIMO is a way to diminish the latency thanks to the beamforming, so that it can reach even the unlucky UEs, having a bad channel quality. However, this property holds for Rayleigh fading channel and we get only approximate favorable propagation in practice. Besides, the BS uses the CSI in order to spatially separate the UEs in UL and DL. This CSI is negatively impacted by the use of non-orthogonal pilots, causing a "pilot contamination problem".

Chapter 3

Cell-free massive MIMO

> *Evolving involves eliminating.*
>
> *Erykah Badu*

Contents

3.1 Introduction

First, this chapter clarifies the paradigm shift from cellular network to cell-free network, especially to give better performance for cell-edge UEs. Later, it presents the incorporation of the massive MIMO technology within the cell-free network, resulting in a cell-free massive MIMO system. Such a system and its basic concepts will be presented in detail. Besides, we will study the channel estimation and the transmission data in UL and DL. For the DL data transmission, the achievable DL rate under sCSI and iCSI will be presented. In addition to that, we will enumerate the practical deployment issues including the radio stripe system and the fronthaul/ backhaul capacity. Finally, some pilot assignment techniques used in cell-free massive MIMO will be defined.

3.2 Paradigm shift from cellular to cell-free networks

In this section, we will explain the key idea behind the paradigm shift crossing from cellular networks into cell-free networks, via multi-cell coordination as follows:

- **Conventional cellular network:** It is designed by dividing the coverage area into many cells. Each one of these cells is equipped with a BS with 1-4 antennas and a UE will be in one of the cells and be served by only that BS, without the cooperation of the other BSs located in other cells, excluding the handover case. In other terms, in this case, we deal with a *single-processed UL/DL data transmission*; see Figure 3.1(a) [10]. In a specific moment, each BS in the cell is surrounded by many active UEs. Data transmissions for UEs in that cell induce interference to UEs belonging to other cells, this phenomenon is called inter-cell interference. To alleviate this problem, relying on beamforming is not sufficient as each BS contains only 1-4 antennas in such system. Spectral efficiency (bit/s/Hz/user) in conventional cellular network can be boosted by integrating the co-processing at many BSs to serve one UE and not to be limited to the BS to which it is connected [46]. This is where the idea of Coordinated Multi-Point (CoMP), detailed as follows, comes in;

- **Coordinated Multi- Point (CoMP):** It is based on co-processing approach. Prior works used other terminologies such as distributed MIMO [47], network MIMO [48, 49] and cooperative multicell MIMO [50]. As a subcategory of CoMP, we cite coordinated multipoint with joint transmission (CoMP-JT) [51,52]. To design such a system,

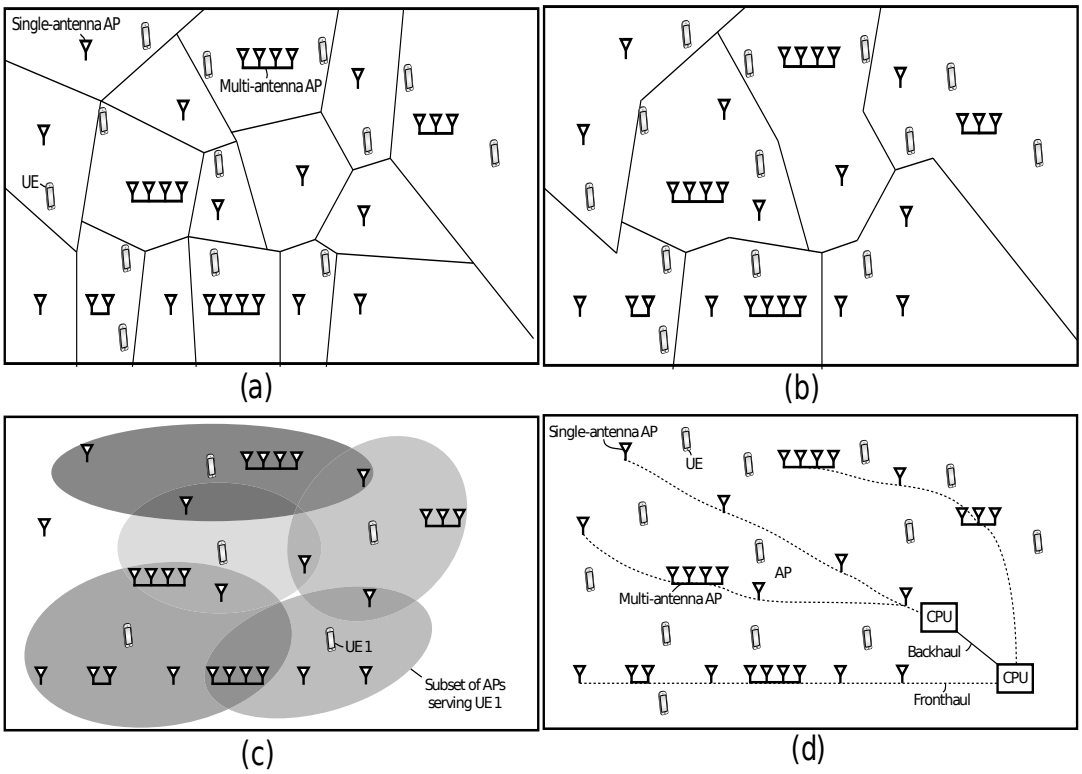

Figure 3.1: With the same collection of APs, we can create many different types of communication networks: (a) A conventional cellular network characterized by the connection of every UE to only one AP.(b) A conventional *network-centric* implementation of CoMP-JT, where the APs form disjoint clusters that act as cells in the sense that the APs in a cluster communicate with the UEs being located in their joint coverage area. (c) In *user-centric networks*, each UE is on communication with a UE-specific subset of the APs. As a result, there are no cell borders and no inter-cell interference in the data transmission. (d) A "cell-free" network permits to implement a *user-centric* network.

we rely on *network-centric policy*. Herein, the APs are clustered in a disjoint way, as depicted in Figure 3.1(b). Each AP of a cluster serves jointly the UEs situated in their commun coverage area. The gains of CoMP-JT in LTE standard obtained theoretically are not as huge as the gains obtained practically [52]. Thus, network-centric approach can not be recommended in practice. It will be wise to design CoMP-JT taking into consideration the practical level, giving the cell free communication in the following parapgrah;

- **Cell-free communication [8, 53]**: The word "cell-free" speaks for itself: there are no cells or borders separating the APs while data transmission. But all the APs herein

work with synergy, via adopting a *user-centric* approach, to serve the UEs. User-centric approach consists in serving a given UE by the closest APs, whilst all APs that induce the interference to that UE, take this issue into consideration.This approach, depicted in Figure 3.1(c), controls the interference, as the APs are more likely closer to the UEs. This improves the quality of the channel estimation. As a consequence, it boosts the accuracy of the beamforming. A more directive and spatially focused beam results in less IUI. Figure 3.1(d) depicted an example of a "cell-free" network, in which the APs are connected via fronthaul cables to CPUs. In case of multiple CPUs, backhaul links are involved to link the CPUs. Later, in terms of IUI especially for cell-edge users, we deal with an example in Figure 3.2 to focus on the reduction of cell edge interference using a "cell-free" network. For further details, it demonstrates the gain achieved for different UE position in a simulation area where 9 APs are distributed in a regular pattern: (a) proves that the spectral efficiencies of cell-edge UEs in a cellular network are poor due to high inter-cell interference; in contrast, (b) proves that a "cell-free" network can circumvent interference especially for cell-edge UEs by allowing co-processing of the APs. In addition to that, this kind of system is still limited by the decay of signal strength with the distance [8].

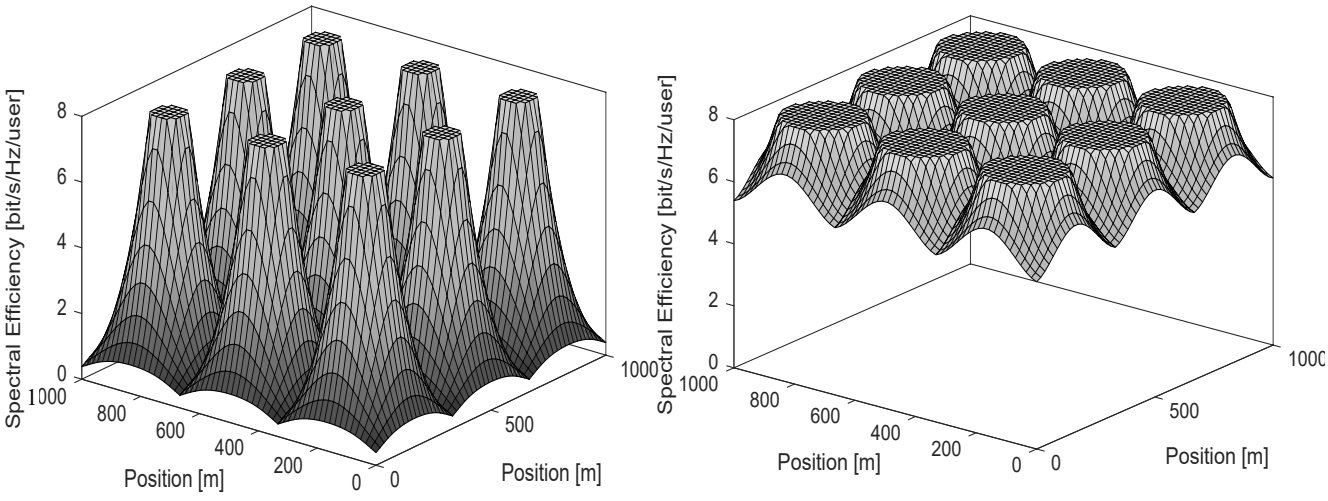

(a) Data coverage in a cellular network.

(b) Data coverage in a "cell-free" network.

Figure 3.2: Spectral efficiency achieved by UEs at different locations. Cell-edge UEs in the cellular network in (a) suffer from poor throughput due to the high inter-cell interference, while the "cell-free" network in (b) is decayed only by the signal strength loss due to the path-loss.

3.3 Cell-free massive MIMO and its features

3.3.1 Cell-free massive MIMO as a way to scaling up CoMP-JT without cells

As we mentioned before, cell free networks suffer from a limited performance of beamforming. As a consequence, the DL signals will not generate beams due to its distributed fashion of APs. Then, in such a system, the CSI is not sufficiently accurate. So how the CSI can be estimated in a cell free network? In that respect, adopting a conventional approach, consisting in sending DL pilots and making the UEs feedback the estimates of the effective DL channel gains, is unscalable as the feedback load depends on the number of APs. To deal with that scalability problem, inspired by [54], the CSI the channel can be estimated locally at each AP. To this end, it is convenient to operate in TDD as the pilot overhead doesn't depend on the number of APS. The CSI between one UE and an AP acquisition herein can be performed by sending a UL pilot by that UE, and then the AP, based on the received signal, estimates its channel to that UE. Thanks to channel reciprocity, the UL channel estimate can be used as DL channel estimate, as it was treated in cellular massive MIMO [5]. Followed by the example of massive MIMO being the way to scale up multi-user MIMO, several works [8, 16, 53] have scaled up the CoMP-JT giving a cell free massive MIMO, where the number of antennas M is very large compared to the number of UEs K ($M \gg K$). The simulation results in [8, 53] demonstrate 5-10 fold improvements compared to cellular networks.

3.3.2 The key properties of cell-free massive MIMO

In this section, we demonstrate the two key properties that make cell-free massive MIMO be efficient, followed by the channel hardening property.

The first property consists in improving spatial multiplexing by increasing the gain, as each UE receives the same signal transmitted from APs situated in different sites by using channels with different characteristics. This property is illustrated in Figure 3.3(a) [8]. It describes cell-free massive MIMO system where the number of APs are 2500 in which we consider 5 and 100m as an inter-site distance. The figure represents the CDF of the channel gain of a UE, where the channel gain vector $\mathbf{g} = [g_1, \cdots, g_M]^T \in \mathbb{C}^M$, where g_m is the channel from the m-th AP to that UE. The channel gain herein is measured by $\max_m |g_m|^2$ in a cellular network, and $||\mathbf{g}||^2$ in "cell-free" massive MIMO. On the one hand, with a large inter-site distance, for the two cases, the UEs with the best channel conditions have similar

channel gains, however the channel gain outperforms, for unlucky UEs, by about 5 dB using "cell-free" massive MIMO system. On the other hand, using a small inter-site distance, all UEs get additional 5-20dB channel gain using "cell-free" massive MIMO system. Added to that, the favorable propagation holds in cell free massive MIMO and the channel vectors of any two UEs, $\mathbf{g}_{\mathrm{UE}_1}$ and $\mathbf{g}_{\mathrm{UE}_2}$, are nearly orthogonal. As in conventional massive MIMO [5], this can remove the IUI. The orthogonality can be evaluted by the squared inner product of the normalized channels as follows

$$\mu_{1,2}^{\mathrm{Orth}} = \frac{|\mathbf{g}_{\mathrm{UE}_1}^{\mathrm{H}} \mathbf{g}_{\mathrm{UE}_2}|^2}{||\mathbf{g}_{\mathrm{UE}_1}||^2 ||\mathbf{g}_{\mathrm{UE}_2}||^2}. \tag{3.1}$$

A greater orthogonality is obtained via a smaller value of $\mu_{1,2}^{\mathrm{Orth}}$. In a cellular network with single-antenna BS, $\mathbf{g}_{\mathrm{UE}_1}$ and $\mathbf{g}_{\mathrm{UE}_2}$ are scalars and thus $\mu_{1,2}^{\mathrm{Orth}}$ is always equal to one. However, favorable propagation holds in "cell-free" Massive MIMO, where $\mathbf{g}_{\mathrm{UE}_1}, \mathbf{g}_{\mathrm{UE}_2} \in \mathbb{C}^M$ [16]. Figure 3.3(b) [8] depicted this property. It represents the CDF of $\mu_{1,2}^{\mathrm{Orth}}$ of 2 UES. The orthogonality measure $\mu_{1,2}^{\mathrm{Orth}}$ is very small for the mentioned inter-site distances. It is to mention that $\mu_{1,2}^{\mathrm{Orth}}$ increases when the inter-site distance reduces, as the pathloss exponent gets smaller when the distance between UE and AP is short.

Added to that, supposing g_{mk} as the channel coefficient between the k-th UE and the m-th AP, the channel hardening in cell-free massive MIMO, defined by ChD_k as follows

$$\mathrm{ChD}_k = 1 - \frac{\mathrm{Var}\left\{\sum_{m=1}^{M} |g_{mk}|^2\right\}}{\left(\mathbb{E}\left\{\sum_{m=1}^{M} |g_{mk}|^2\right\}\right)^2}, \tag{3.2}$$

is less accentuated compared to cellular massive MIMO, as it is depicted in Figure 3.4 in [14]. The more ChD_k gets larger, the more the channel hardens for the k-th UE, as if it were determinist.

3.4 Cell-free massive MIMO system model

In this work, we adopt the same system model for cell-free massive MIMO system as in [8], [14], and [55]. It consists of M single-antenna APs and K single-antenna UEs, which are deployed randomly in a large space without boundaries with $M \gg K$. The APs are connected to one or more CPUs through a fronthaul network and the CPUs are connected

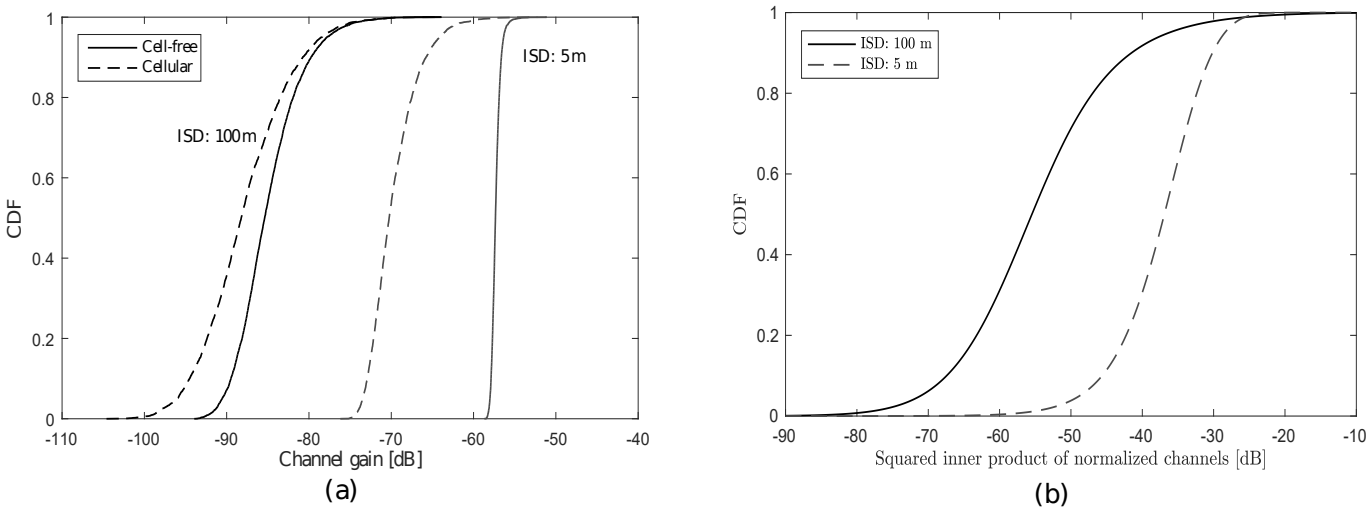

Figure 3.3: Two key features that make cell-free Massive MIMO recommended. (a) The distribution of the channel gain is more beneficial than in a cellular system, thanks to the additional macro-diversity; (b) The inner product of the channel vectors of two randomly selected UEs is very small, which is called *favorable propagation*. The simulation setup considers 2500 single antenna APs deployed on a square grid with wrap-around and varying inter-site distance (ISD).

via backhaul network as it is shown in Figure 3.5. The features of this system are as follows: the M APs communicate simultaneously with the K UEs in the same time/frequency resource.

The half duplexing used is TDD, allowing one directed communication at a time slot, either from the APs to UEs (DL) or from UEs to APs (UL). As a consequence, the system takes advantage from channel reciprocity, i.e., the channel response in the UL and in the DL are the same. This requires a calibration of the hardware chains. As a DL precoding technique, we use the conjugate beamforming, also known maximum-ratio transmission (MRT). The choice of such a precoder is justified due to the following features:

(i) Its ability to be implemented on a distributed system [32];

(ii) To avoid the exchange of CSI among APs;

(iii) To reduce the fronthaul network load [10] because it requires CSI acquisition and the precoding to be performed locally at each AP by exploiting the channel reciprocity in TDD system;

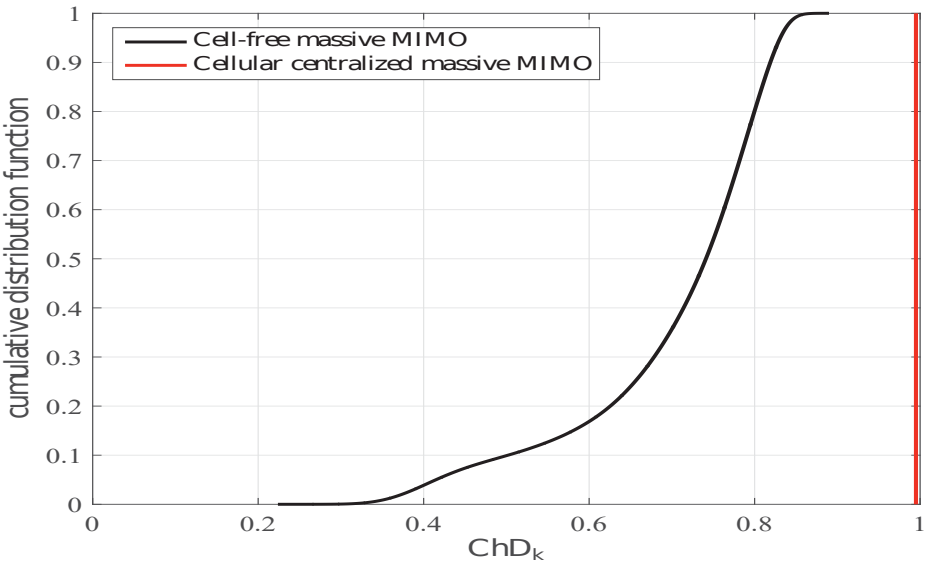

Figure 3.4: In CF massive MIMO networks, the ChD, the channel hardening degree, is much lower compared to one in conventional massive MIMO. In this system, we assume 200 APs randomly distributed in an area of 1 km2, and i.i.d. Rayleigh fading channel.

(iv) It is not considered as an optimal precoder but it is a low-complexity precoder and composed of inexpensive hardware components.

Following the system model in [14], we assume that TDD frame length is equal to the coherence interval. As a consequence, the channel is considered static within a frame and variable independently for each frame. We consider g_{mk} the channel coefficient between the k-th UE and the m-th AP, defined as follows

$$g_{mk} = \beta_{mk}^{1/2} h_{mk}, \tag{3.3}$$

where the h_{mk} term describes the small-scale fading, and the β_{mk} term describes the large-scale fading, which incorporates pathloss and shadowing. We suppose that h_{mk}, $m = 1, \ldots, M$, $k = 1, \ldots, K$, are independent and identically distributed (i.i.d.) $\mathcal{CN}(0, 1)$ RVs. The assumption of independent small-scale fading is justified by the fact that the APs and the UEs are deployed in a large area. As a consequence, the scatterers of each AP and each UE are different. Added to that, the small-scale fading is supposed to be static during each coherence interval and change independently from one coherence interval to another. The large-scale fading changes much more slowly, and stays constant for several coherence in-

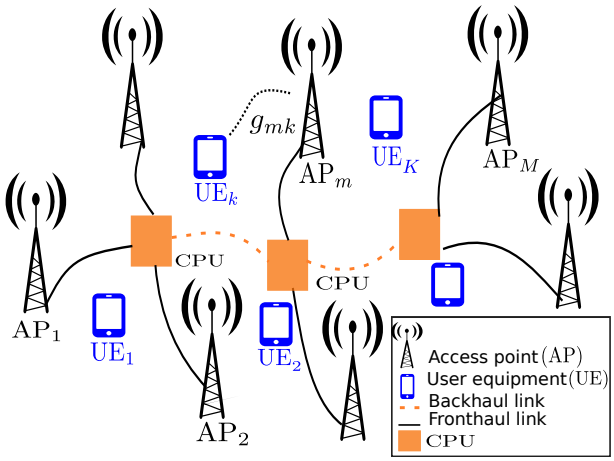

Figure 3.5: Cell-free massive MIMO architecture.

tervals. Hence, the $\{\beta_{mk}\}$ coefficients are supposed to be known.

3.4.1 UL training

In our case, as we supposed that the channel coherence interval is equal to a TDD frame, we have $\tau_{\text{ul,p}} < \tau_{\text{c}}$. Getting inspired by [55], we consider the UL pilot sequence of length $\tau_{\text{ul,p}}$ samples sent by the k-th UE as $\sqrt{\tau_{\text{ul,p}}}\boldsymbol{\varphi}_k \in \mathbb{C}^{\tau_{\text{ul,p}}\times 1}$, $k = 1, \ldots, K$. During training phase, we suppose that the pilot sequences are transmitted with full power, and are mutually orthonormal. To this end, one of the sine qua non conditions is that $\tau_{\text{ul,p}} \geqslant K$, i.e., $\tau_{\text{ul,p}} = K$ is the smallest number of symbols required to generate K orthogonal vectors. The m-th AP receives K UL pilots from all UEs as follows

$$\boldsymbol{y}_{\text{ul,p},m} = \sqrt{\tau_{\text{ul,p}}\rho_{\text{ul,p}}} \sum_{k=1}^{K} g_{mk}\boldsymbol{\varphi}_k + \boldsymbol{w}_{\text{ul,p},m}, \tag{3.4}$$

where $\rho_{\text{ul,p}}$ is the normalized transmit signal-to-noise ratio (SNR) related to the pilot symbol and $\boldsymbol{w}_{\text{ul,p},m}$ is the additive noise vector, whose elements are i.i.d. $\mathcal{CN}(0,1)$ RVs. To estimate g_{mk}, we follow these instructions: (i) the m-th AP projects the received pilot signal $\boldsymbol{y}_{\text{ul,p},m}$ onto $\boldsymbol{\varphi}_k$ giving $\tilde{y}_{\text{ul,p},mk}$ as:

$$\tilde{y}_{\text{ul,p},mk} = \boldsymbol{\varphi}_k^H \boldsymbol{y}_{\text{ul,p},m} = \sqrt{\tau_{\text{ul,p}}\rho_{\text{ul,p}}} g_{mk} + \boldsymbol{\varphi}_k^H \boldsymbol{w}_{\text{ul,p},m}, \tag{3.5}$$

and; (ii) the resulted signal $\tilde{y}_{\text{ul,p},mk}$ is then used as a prior information to perform the minimum mean square error (MMSE) estimation of g_{mk} giving $\hat{g}_{mk}$, $k = 1, \ldots, K$ as follows

$$\hat{g}_{mk} = \frac{\mathbb{E}\{\tilde{y}^*_{\text{ul,p},m} g_{mk}\}}{\mathbb{E}\{|\tilde{y}_{\text{ul,p},m}|^2\}} \tilde{y}_{\text{ul,p},m} = c_{mk} \tilde{y}_{\text{ul,p},m} \text{ (the proof is in Appendex B.1)}, \tag{3.6}$$

where

$$c_{mk} \triangleq \frac{\sqrt{\tau_{\text{ul,p}} \rho_{\text{ul,p}}} \beta_{mk}}{\tau_{\text{ul,p}} \rho_{\text{ul,p}} \beta_{mk} + 1}. \tag{3.7}$$

The channel estimation error is given by $\tilde{g}_{mk} \triangleq g_{mk} - \hat{g}_{mk}$. By definition, $\hat{g}_{mk}$ and $\tilde{g}_{mk}$ are uncorrelated, owing on the linear MMSE properties [56]. Furthermore, the estimate and the estimation error are jointly Gaussian distributed, thus they are statistically independent. We denote by γ_{mk} the variance of the channel estimate described as follows

$$\gamma_{mk} \triangleq \mathbb{E}\{|\hat{g}_{mk}|^2\} = \sqrt{\tau_{\text{ul,p}} \rho_{\text{ul,p}}} \beta_{mk} c_{mk} \text{ (the proof is in Appendex B.2)}. \tag{3.8}$$

The channel estimate and the estimation error in UL, respectively, are distributed as $\hat{g}_{mk} \sim \mathcal{CN}(0, \gamma_{mk})$ and $\tilde{g}_{mk} \sim \mathcal{CN}(0, \beta_{mk} - \gamma_{mk})$.

3.4.2 DL payload data transmission

In the DL data transmission phase, each AP implements a power control, and uses the UL estimated CSI in order to precode, via a conjugate beamforming, the signals to be transmitted to all the K UEs. Hence, as it is described on the AP side in Figure 3.6, the m-th AP transmits to all UEs the following signal:

$$x^{\text{CF}}_{\text{dl,d},m} = \sqrt{\rho_{\text{dl,d}}} \sum_{k=1}^{K} \sqrt{\eta_{mk}} \hat{g}^*_{mk} q_k, \tag{3.9}$$

where q_k is the data symbol intended for the k-th UE, which satisfies $\mathbb{E}\{|q_k|^2\} = 1$. q_k are zero-mean and unit-variance symbols. Furthermore, they are uncorrelated. $\rho_{\text{dl,d}}$ is the normalized transmit SNR corresponding to the data symbol. Added to that, η_{mk}, $m = 1, \ldots, M$,$k = 1, \ldots, K$, are the power control coefficients, which represent the power transmitted by the m-th AP for the k-th UE. They are fixed subject to the average power constraint at each AP:

$$\mathbb{E}\{|x^{\text{CF}}_{\text{dl,d},m}|^2\} \leqslant \rho_{\text{dl,d}}. \tag{3.10}$$

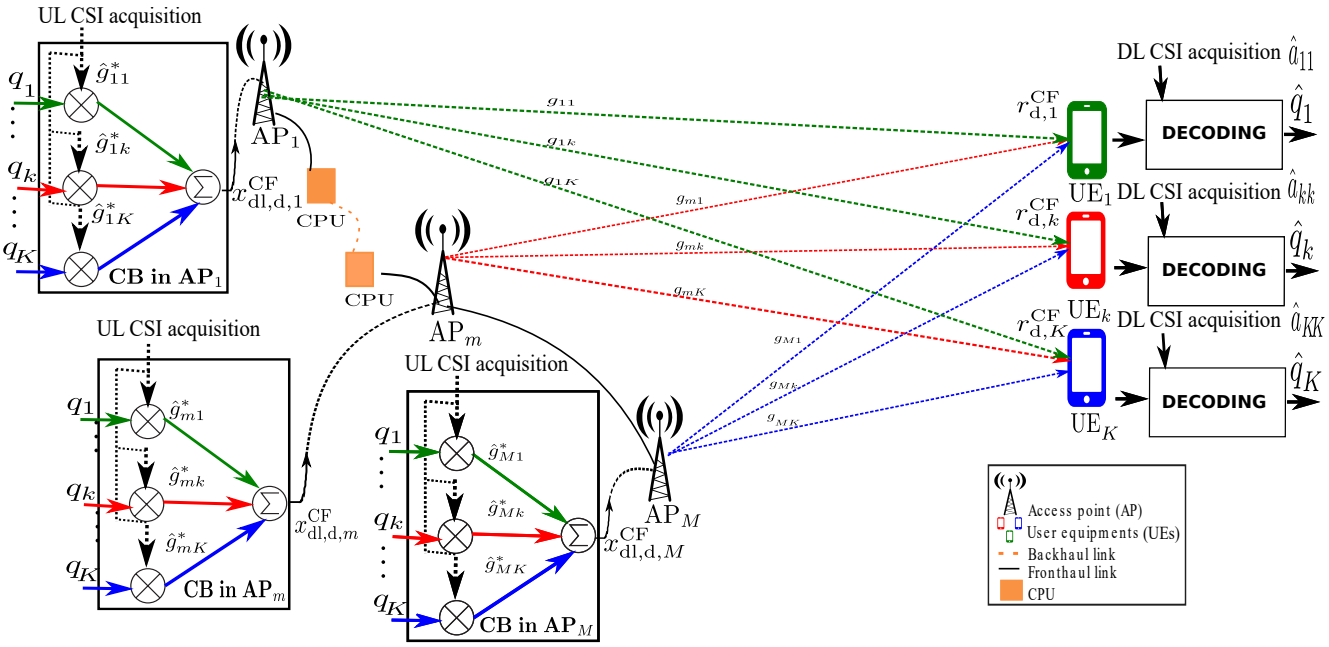

Figure 3.6: DL Data transmission in cell-free massive MIMO with conjugate beamforming (CB) in each AP (power control is not mentioned in the figure).

The power constraint (3.10) can be given as a function of η_{mk}, $m = 1, ..., M, k = 1, ..., K$, and γ_{mk} when we substitute (3.9) into (3.10) as follows

$$\sum_{k=1}^{K} \eta_{mk} \gamma_{mk} \leqslant 1 \quad \forall m \tag{3.11}$$

The k-th UE receives a linear combination of the data signals transmitted by all the APs in (3.9) as follows

$$r_{\mathrm{d},k}^{\mathrm{CF}} = \sum_{m=1}^{M} g_{mk} x_{\mathrm{dl,d},m}^{\mathrm{CF}} + w_{\mathrm{dl},k}; \tag{3.12}$$

$$= \sqrt{\rho_{\mathrm{dl,d}}} \sum_{k'=1}^{K} a_{kk'} q_{k'} + w_{\mathrm{dl,d},k}; \tag{3.13}$$

$$= \underbrace{\sqrt{\rho_{\mathrm{dl,d}}} a_{kk} q_k}_{\text{desired signal}} + \underbrace{\sqrt{\rho_{\mathrm{dl,d}}} \sum_{k' \neq k}^{K} a_{kk'} q_{k'}}_{\text{IUI}} + \underbrace{w_{\mathrm{dl,d},k}}_{\text{noise}}, \tag{3.14}$$

where $a_{kk'} \triangleq \sum_{m=1}^{M} \sqrt{\eta_{mk'}} g_{mk} \hat{g}^{*}_{mk'}, k' = 1, \ldots, K$, describes the effective DL channel gain seen by the k-th UE for the transmitted symbol to the k'-th UE and $w_{\text{dl,d},k}$ is additive $\mathcal{CN}(0,1)$ noise at the k-th UE. It is primordial that the k-th UE must have a sufficient knowledge of a_{kk} in order to reliably decode q_k [55], as it is revealed on the UE side in the decoding block in Figure 3.6. To this end, among the methods used, the k-th UE can rely on channel hardening and assume that $a_{kk} \approx \mathbb{E}\{a_{kk}\}$. This method is appreciated for conventional massive MIMO because of the law of the large numbers. But, it is not the case for cell-free massive MIMO because of its distributed architecture. In fact, only a subset of APs, i.e., the closest APs can serve a UE because the far ones are attenuated by larger path-loss. Furthermore, the k-th UE can use DL beamformed pilots to estimate a_{kk}.

3.4.3 DL training

Similar to [55], in order to determine the effective DL channel gain estimate $\hat{a}_{kk}$, the m-th AP precodes, via the conjugate beamforming, and beamforms to all UEs the DL pilots defined by $\sqrt{\tau_{\text{dl,p}}}\boldsymbol{\psi}_{k'} \in \mathbb{C}^{\tau_{\text{dl,p}} \times 1}$, $k' = 1, \ldots, K$. Hence, the $\tau_{\text{dl,p}} \times 1$-size pilot signal $x^{\text{CF}}_{\text{dl,p},m}$ sent from the m-th AP, is given by

$$\boldsymbol{x}^{\text{CF}}_{\text{dl,p},m} = \sqrt{\tau_{\text{dl,p}} \rho_{\text{dl,p}}} \sum_{k'=1}^{K} \sqrt{\eta_{mk'}} \hat{g}^{*}_{mk'} \boldsymbol{\psi}_{k'}, \tag{3.15}$$

where $\rho_{\text{dl,p}}$ is the normalized transmit SNR per DL pilot symbol and $\boldsymbol{\psi}_1 \ldots \boldsymbol{\psi}_K$ are assigned randomly from a set of orthogonal sequences of length $\tau_{\text{dl,p}} < K$ [8]. Hence, the DL pilot sequences can be either mutually orthonormal or identical as follows

$$\boldsymbol{\psi}_k^H \boldsymbol{\psi}_{k'} = \begin{cases} 1, & \text{if } \boldsymbol{\psi}_k = \boldsymbol{\psi}_{k'}, \\ 0, & \text{otherwise.} \end{cases} \tag{3.16}$$

The k-th UE receives a corresponding $\tau_{\text{dl,p}} \times 1$ pilot vector as follows

$$\boldsymbol{y}_{\text{dl,p},k} = \sqrt{\tau_{\text{dl,p}} \rho_{\text{dl,p}}} \sum_{k'=1}^{K} a_{kk'} \boldsymbol{\psi}_{k'} + \boldsymbol{w}_{\text{dl,p},k}, \tag{3.17}$$

where $\boldsymbol{w}_{\text{dl,p},k}$ is a receiver noise vector, whose elements are i.i.d $\mathcal{CN}(0,1)$ RVs.
In order to estimate the effective DL channel gain $\hat{a}_{kk}$, we follow this process. The k-th UE

projects the received DL pilot onto the pilot sequence $\boldsymbol{\psi}_k^H$ as follows:

$$\tilde{y}_{\text{dl,p},k} = \boldsymbol{\psi}_k^H \boldsymbol{y}_{\text{dl,p},k} \ , \tag{3.18}$$

$$= \sqrt{\tau_{\text{dl,p}}\rho_{\text{dl,p}}} a_{kk} + \sum_{k' \neq k}^{K} a_{kk'} \boldsymbol{\psi}_k^H \boldsymbol{\psi}_{k'} + n_{\text{dl,p},k} \ , \tag{3.19}$$

where $n_{\text{dl,p},k} \triangleq \boldsymbol{\psi}_k^H \boldsymbol{w}_{\text{dl,p},k} \sim \mathcal{CN}(0,1)$. The second term in (3.19) describes the DL pilot contamination effect. Based on [56], the resulted signal $\tilde{y}_{\text{dl,p},k}$ is then used as a prior information to perform MMSE estimation of a_{kk} getting $\hat{a}_{kk}$, $k = 1, \ldots, K$ as follows

$$\hat{a}_{kk} = \mathbb{E}\{a_{kk}\} + \frac{\text{Cov}\{a_{kk}, \tilde{y}_{\text{dl,p},k}\}}{\text{Cov}\{\tilde{y}_{\text{dl,p},k}, \tilde{y}_{\text{dl,p},k}\}} (\tilde{y}_{\text{dl,p},k} - \mathbb{E}\{\tilde{y}_{\text{dl,p},k}\}); \tag{3.20}$$

$$= \mathbb{E}\left\{a_{kk}\right\} + \frac{\sqrt{\tau_{\text{dl,p}}\rho_{\text{dl,p}}}\,\text{Var}\left\{a_{kk}\right\}}{\tau_{\text{dl,p}}\rho_{\text{dl,p}}\,\text{Var}\left\{a_{kk}\right\} + 1} \left(\tilde{y}_{\text{dl,p},k} - \sqrt{\tau_{\text{dl,p}}\rho_{\text{dl,p}}}\mathbb{E}\left\{a_{kk}\right\}\right); \tag{3.21}$$

$$= \frac{\sqrt{\tau_{\text{d,p}}\rho_{\text{dl,p}}}\zeta_{kk}\tilde{y}_{\text{dl,p},k} + \sum_{m=1}^{M}\sqrt{\eta_{mk}}\gamma_{mk}}{\tau_{\text{dl,p}}\rho_{\text{dl},p}\zeta_{kk} + 1}, \tag{3.22}$$

where $\zeta_{kk} \triangleq \sum_{m=1}^{M} \eta_{mk}\beta_{mk}\gamma_{mk}$ and $\hat{a}_{kk}$ is used by the k-th UE to decode its intended data as it is described on the UE side in Figure 3.6. The proof to calculate $\hat{a}_{kk}$ is shown in detail in [15, 55]. The estimation error is as follows: $\tilde{a}_{kk} = a_{kk} - \hat{a}_{kk}$.

3.5 Performance analysis

We consider two types of CSIs namely: instantaneous CSI (iCSI) and statistical CSI (sCSI) [57]. In iCSI, the current or instantaneous channel conditions are known. In sCSI, we have access to the statistical characterizations of the channel. The CSI acquisition depends on the speed of channel variation as follows:

- In fast fading channels, where channel conditions vary rapidly, only sCSI is suitable.
- In slow fading channels, iCSI can be estimated in much larger coherence intervals with some estimation errors before being changed.

In practice, the CSI often lies in between sCSI and iCSI. For example, [14] considered a pilot utility metric and compared it to a specific threshold to decide whether the UE can rely on iCSI or on sCSI to decode data. In what follows, we focus on studying the achievable DL rate under sCSI and iCSI.

$$R_k^{\text{iCSI,CF}} = \log_2(1 + \frac{\overbrace{\rho_{\text{dl,d}}\left(\sum_{m=1}^{M}\sqrt{\eta_{mk}}\gamma_{mk}\right)^2}^{W_{\text{DS}_k}} + \rho_{\text{dl,d}}\kappa_k}{\underbrace{\rho_{\text{dl,d}}(\zeta_{kk} - \kappa_k)}_{V_{a_{kk}}} + \sum_{k'\neq k}^{K}\underbrace{\rho_{\text{dl,d}}\zeta_{kk'}}_{W_{\text{IUI}_{kk'}}} + 1}) \tag{3.23}$$

$$R_k^{\text{sCSI,CF}} = \log_2(1 + \frac{\rho_{\text{dl,d}}\left(\sum_{m=1}^{M}\sqrt{\eta_{mk}}\gamma_{mk}\right)^2}{\rho_{\text{dl,d}}\zeta_{kk} + \sum_{k'\neq k}^{K}\rho_{\text{dl,d}}\zeta_{kk'} + 1}) \tag{3.24}$$

3.5.1 Achievable DL rate under instantaneous CSI

Let's consider the following hypothesis, dealing with a fading channel with a non-Gaussian noise and a UE having an imperfect iCSI. According to these hypotheses, the UE relies on beamformed DL pilots and estimates the DL channel gain. This latter is considered as a prior information for the capacity-bounding technique by following the same process as [5, Sec. 2.3.5] and [15, Sec. III-A]. As $\{a_{kk'}\}, k, k' = 1, \ldots, K$, can be approximated as Gaussian random variables, the DL ergodic capacity lower bound can be approximated by the following proposition:

Proposition 1: A closed-form expression for an approximate achievable downlink rate of the transmission from the APs to the k-th UE in a CF-mMIMO system with conjugate beamforming, orthogonal UL and non-orthogonal DL pilots, for any finite M and K, is given by (3.23) on the top of the next page. It is a special case of [15, Eq. 32] where the UL pilots φ_k are orthogonal. We note that in (3.23) we have,

$$\kappa_k = \text{Var}\{\hat{a}_{kk}\} = \frac{\tau_{\text{dl,p}}\rho_{\text{dl,p}}\zeta_{kk}^2}{1 + \tau_{\text{dl,p}}\rho_{\text{dl,p}}\sum_{k'=1}^{K}\zeta_{kk'}|\boldsymbol{\psi}_k^H\boldsymbol{\psi}_{k'}|^2}, \tag{3.25}$$

where $\zeta_{kk'} = \sum_{m=1}^{M}\eta_{mk'}\beta_{mk}\gamma_{mk'}$. κ_k is the variance of the DL channel estimate $\hat{a}_{kk}$, which includes the effects of the DL pilot contamination. It represents the DL counterpart

of the term γ_{mk}. In what follows, we extract the following terms from (3.23):

$$W_{\mathrm{DS}_k} = \rho_{\mathrm{dl,d}} \left(\sum_{m=1}^{M} \sqrt{\eta_{mk}} \gamma_{mk} \right)^2 + \rho_{\mathrm{dl,d}} \kappa_k, \tag{3.26}$$

$$W_{\mathrm{IUI}_{kk'}} = \rho_{\mathrm{dl,d}} \zeta_{kk'}, \tag{3.27}$$

$$V_{\tilde{a}_{kk}} = \rho_{\mathrm{dl,d}} (\zeta_{kk} - \kappa_k). \tag{3.28}$$

These terms represent, respectively, the power of the desired signal, the IUI caused by the k'-th UE and the variance of the DL channel estimation error $\tilde{a}_{kk}$. The proof of this proposition can be found in [15], while considering orthogonal UL pilots φ_k.

3.5.2 Achievable DL rate under statistical channel at the receiver

We suppose that the k-th UE relies on sCSI. As a consequence, getting inspired by [15, Eq. 36] and [5, Sec. 2.3.4], the achievable DL rate denoted as $R_k^{\mathrm{sCSI,CF}}$, is given by (3.24) on the top of the page. The term $\rho_{\mathrm{dl,p}} \zeta_{kk'}$ represents the beamforming gain uncertainty. It originates from the UEs' absence of iCSI. As it is shown in (3.28), the beamforming gain uncertainty represents not only the variance of the effective DL channel, but also it gives an indirect measure of the channel hardening. Precisely, it is inversely proportional to the channel hardening degree [14]. The equation (3.28) can be proved using *use-and-forget* technique in [15].

3.6 Practical deployment issues

3.6.1 Radio stripe system

To deploy cell-free massive MIMO, we need a lot of meters of cables to connect the APs to the CPU, as a result it forms a « spaghetti monster ». Added to that, we will probably need even more antennas than centralized massive MIMO, it's not enough to take the antennas from centralized MIMO and spread the same number of them out. Because there were good reasons to put BSs up in towers over the roof. In centralized MIMO, we can see above different obstacles and we can send signals over the roof of a building to reach the next building. While that will not be possible when the antennas are distributed at street level close to the UEs. Then, we will need to put out more antennas. Another complications are when it comes to complexity how we control processing in a good way in terms of the

time and how we take care of all the computation of all the signals to gather in CPU. An alternative to deal with that problem is the radio stripes. Its idea is to connect one AP to a CPU instead of putting a passive cable there but putting a lot of antennas within the cable and turning the entire cable into a part of a network architecture.

The radio stripe, as depicted in Figure 3.7 [10] is based on a long stripe composed a cable containing antennas and each antenna is connected to an antenna processing unit (APU) that is containing all of the Harware component (filters, A/D and D/A converters, power amplifiers, phase shifters, filters, modulators). The question is how can we put all these components into a cable when the BS is large. We could apply what we did in a mobile phone based on very small chipsets and do that instead of using this high power advanced equipment that we have been using in the BSs in the past. For example, if the carrier frequency is 5.2 GHz which is a typical bound for 5G, then the $\frac{\lambda}{2}$ antenna size is 2.8 cm. Thus, the antennas and processing hardware can be easily fitted in a cable/stripe. Each radio stripe is then connected to one or multiple CPUs. The receive/transmit processing of an antenna is performed right next to itself. Since the total number of distributed antennas is supposed to be tremendous, the antenna transmit power is likely to be very modest. As a consequence, it results in low dissipation of heat, small volume and weight, and low cost. Moreveor, radio stripe is highly robust as just few APUs can break with only a limited impact on the network. An example of an application of radio stripe is in Figure 3.8 [10].

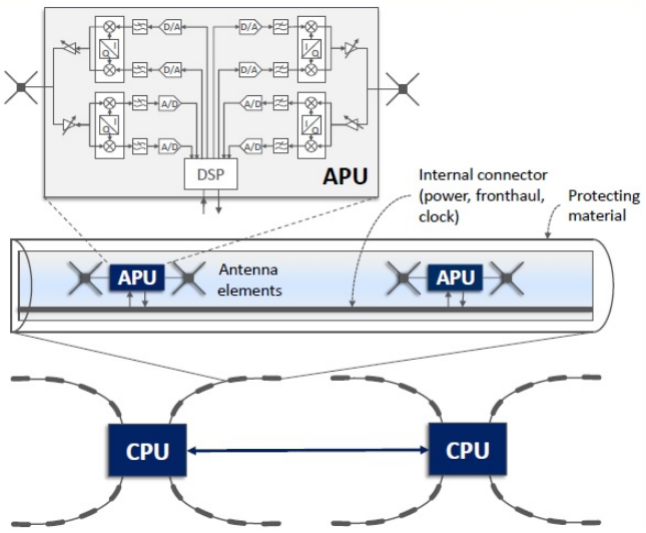

Figure 3.7: Example of a radio stripe system.

Figure 3.8: Radio stripes, shown with red dots, are mounted in an invisible way in constructions.

3.6.2 Fronthaul and backhaul capacity

As the share of CSI between antenna elements in "cell-free" Massive MIMO is not required, the CPUs must provide each APU with the data streams that its antenna elements will transmit. The data is transmitted from the core network via the backhaul links and then forwarded to the APU over the fronthaul links; see Figure 3.8. Similarly, the CPU will receive the resulted signals from its radio stripes over the fronthaul and decode the data streams. These latters will then be transmitted to the core network via the backhaul links.

The fronthaul capacity needed in a radio stripe is proportional to the number of simultaneous data streams that it could spatially multiplex at maximum network load. The backhaul capacity required corresponds to the sum rate of the data streams that the radio stripes linked to the CPU will transmit/receive at maximum network load. To address the limitation of the capacity requirements, it is to reduce the number of UEs that can be served per AP (e.g., radio stripe) and CPU. To prevent forming cell borders, a *user-centric* perspective must be utilized when choosing which subset of APs is dedicated to serve a particular UE, as illustrated in Figure 3.1(c). [58] considers to select the 95%-subsets that maximize the energy efficiency of the network, taking into account the power consumption of backhaul signaling.

3.6.3 Power control

Among the power control policy, we cite max-min fairness power control. The goal of such power control policy is to deliver the same spectral efficiency to all UEs and making that spectral efficiency as large as possible, leading to a uniformly good UE service in the

network. In practice, some UEs might have bad channels to all APs, due to unlucky pathloss and shadowing. With max-min fairness power control, substantial power has to be allocated to these UEs and the spectral efficiency might still be low, leading to a bad service for everyone. Therefore, some deeply shadowed UEs need to be dropped from service to ensure a uniformly good service to all others. In other terms, the rate of the smaller (minimized) flows that is made as large as possible. The max-min fairness (maximized) by the algorithm, yiels higher relative priority to small flows. This power-control algorithm has been used in [8].

3.6.4 Pilot assignment

To mitigate the pilot contamination issue, pilot assignment schemes should be applied to get better performance. Later, we enumerate some common pilot assignment schemes applied in the litterature in "cell-free" Massive MIMO:

- **Random pilot assignment:** It consists in assigning to each UE a pilot randomly from a set of mutually orthogonal pilot sequences. This approach seems to be easy in terms of implementation, but the UEs in close vicinity are likely to reuse the same pilot, this causes a bad performance of the system by a high contamination problem [8, 59, 60];

- **Greedy pilot assignment:** In [8] uses a greedy pilot assignment as follows. It assumes that the UL pilots $\boldsymbol{\varphi_k}, k = \{1 \cdots K\}$ are mutually non-orthogonal. Initially, it consists of assigning random UL pilot to all UEs based on the random pilot assignment strategy. First, it is to find the UE k^* having the worst DL rate per UE $R^{\mathrm{CF}}_{\mathrm{dl},k}$ as follows

$$k^* = \arg\min_k R^{\mathrm{CF}}_{\mathrm{dl},k}. \tag{3.29}$$

  Second, it is to update the assignment of a new pilot to that UE chosen previously, k^*, $\boldsymbol{\varphi_{k^*}}$ such that the UL pilot contamination effect, measured by

$$\sum_{m=1}^{M} \sum_{k' \neq k^*}^{K} \beta_{mk'} \left| \boldsymbol{\varphi}_{\boldsymbol{k^*}}^H \boldsymbol{\varphi_{k'}} \right|^2, \tag{3.30}$$

  is minimized. The first and second steps are repeated until the algorithm reaches a predefined number of iterations.

  Furthermore, [15] uses a greedy pilot assignment algorithm to assign jointly UL pi-

lots, $\boldsymbol{\varphi}_k$, and DL pilots, $\boldsymbol{\psi}_k$, based on minimizing a utility function, which takes into consideration the UL and DL pilot contamination issue as follows

$$f\left(k, \{\boldsymbol{\varphi}_k, \boldsymbol{\psi}_k\}\right) = \sum_{m=1}^{M} \sum_{k' \neq k}^{K} \left(\beta_{mk'} \left| \boldsymbol{\varphi}_k^{\mathrm{H}} \boldsymbol{\varphi}_{k'} \right|^2 + \eta_{mk'} \beta_{mk} \gamma_{mk'} \left| \boldsymbol{\psi}_k^{\mathrm{H}} \boldsymbol{\psi}_{k'} \right|^2 \right). \quad (3.31)$$

- **Brute-force assignment:** It consists in exhaustive search over all possible combinations of pilot sequences in order to maximize a utility function such as the total of spectral efficiency or the max-min spectral efficiency. This brute-force algorithm provides an optimal solution but its complexity increases as the number of UEs gets higher [10].

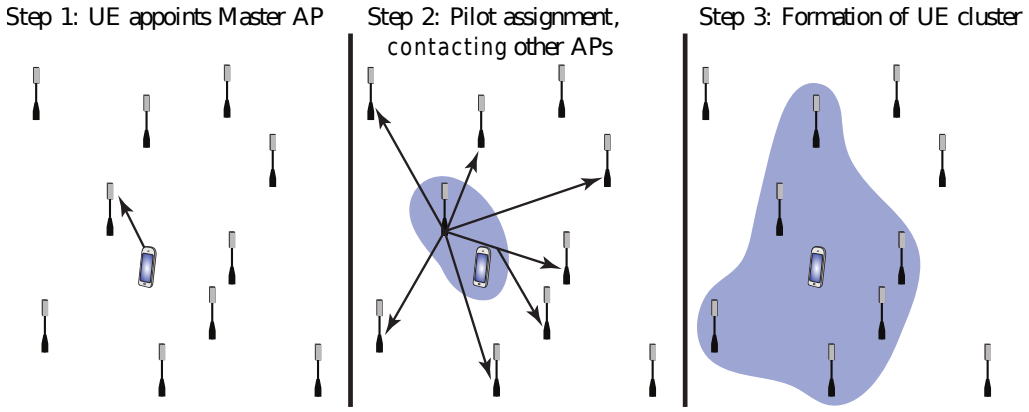

Figure 3.9: Main steps of *dynamic cooperation clustering* algorithm.

- **Structured/clustering pilot assignment**: A dynamic pilot reuse (DPR) method is proposed to permit a single pilot to be shared between a pair of UEs in cell-free massive MIMO [61]. Furthermore, a *dynamic cooperation algorithm* is proposed in [62]. Herein the algorithm is called dynamic because if the UEs are moving around, the APs that serve the UEs change. Three steps of this algorithm can be described as follows in Figure 3.9 [62]. First, a UE gets access to the network by sending a random access request that can reach the strongest (by a listening signal sent in DL). Based on that, the UE appoints a master AP that is responsible for serving this UE. Then, this master AP picks a pilot that this UE can use, minimizing the pilot contamination problem. The Master AP contacts all the APs that are in the neighboring area and informs them that the lastly picked pilot is used to serve that UE and proposes them

to join it to serve that UE. Finally, some of the APs agree to serve that UE forming a cluster of AP serving that UE as they offer good channel conditions.

To achieve better network performance, the pilot assignment strategies can be combined with the power control policies.

3.7 Conclusion

In this chapter, we explained the paradigm shift from cellular to cell-free networks, which is mainly to offer a better performance to cell-edge UEs in massive MIMO in cellular networks. Later, we especially presented an overview in cell-free massive MIMO. We were laser-focused on the DL data transmission, and on the UL/DL channel estimation, based on orthogonal pilot assignment for the UL and non-orthogonal pilot assignment for the DL. From the DL data transmission, we deduced a closed form of the achievable DL rate under sCSI and iCSI. Further discussion about the practical issues in cell-free massive MIMO were included such as the pilot assignment policies and backhaul and fronthaul capacity in cell-free massive MIMO system. Added to that, the non-orthogonal pilot assignment for the DL channel estimation triggers a problem called « DL pilot contamination » in cell-free massive MIMO. This issue is mitigated through our approach, which is a DL pilot assignment based on coloring graph. Our contribution is treated in details in the next chapter.

Chapter 4

Graph coloring for DL pilot assignment in cell-free massive MIMO

> “I found I could say things with color and shapes that I couldn’t say any other way - things I had no words for.
>
> *Georgia O’Keeffe* ”

Contents

4.1 Introduction

In this chapter, we will introduce our contribution, which consists in using a graph theoretic approach for DL pilot assignment. Being aware of resource waste by using DL pilots, we will present an algorithm to reduce the DL pilot overhead while considering the DL contamination problem. Later, we evaluate the improvement of the performance of our proposed algorithm compared to prior works in cell-free massive MIMO by a quantitative study.

4.2 Graph theoretic approach for DL pilot assignment

In essence, we deal with the proposed graph-theoretic approach to allocate DL training resources to all UEs in cell-free massive MIMO. First, we explain the idea behind the proposed approach and, then, the graph-theoretic approach is deployed in details to assign pilots.

As it is shown in equation (3.23), the DL achievable rate $R_k^{\text{iCSI,CF}}$ depends on κ_k, which is limited by the DL pilot contamination. To illustrate this problem, we deal with an example in Figure 4.1(a). The UEs, painted with the same color, share the same beamformed DL pilot. Thus, these UEs, in the red shadow zone, suffer from a severe pilot contamination. From equation (3.23), it is intuitive that $\sum_{k' \neq k}^{K} \text{W}_{\text{IUI}_{kk'}}$ represents the interference strength from other UEs applied to the k-UE. Hence, we define a symmetric matrix $\Theta = [\theta_{kk'}]_{K \times K}$, whose elements measure the strength of potential IUI between the k-th UE and the k'-th UE and are defined as follows

$$\theta_{kk'} = \frac{W_{\text{IUI}_{kk'}}}{W_{\text{DS}_k}} + \frac{W_{\text{IUI}_{k'k}}}{W_{\text{DS}_{k'}}}. \tag{4.1}$$

θ is expressly the ratio of interference channel strength and the desired signal strength. Larger $\theta_{kk'}$ indicates more severe interference between the k-th and the k'-th UEs when the same DL pilot is allocated to these UEs. Il will be wise to define a threshold λ_{th} by which we can decide whether two UEs can reuse the same pilot, i.e., $\theta_{k,k'} < \lambda_{\text{th}}$, or not.

4.2.1 Construction of conflict graph based pilot allocation

In this section, we describe a resource-allocation approach, which exploits the knowledge of dominant DL interference. The proposed method converts the resource allocation problem into a graph coloring problem.

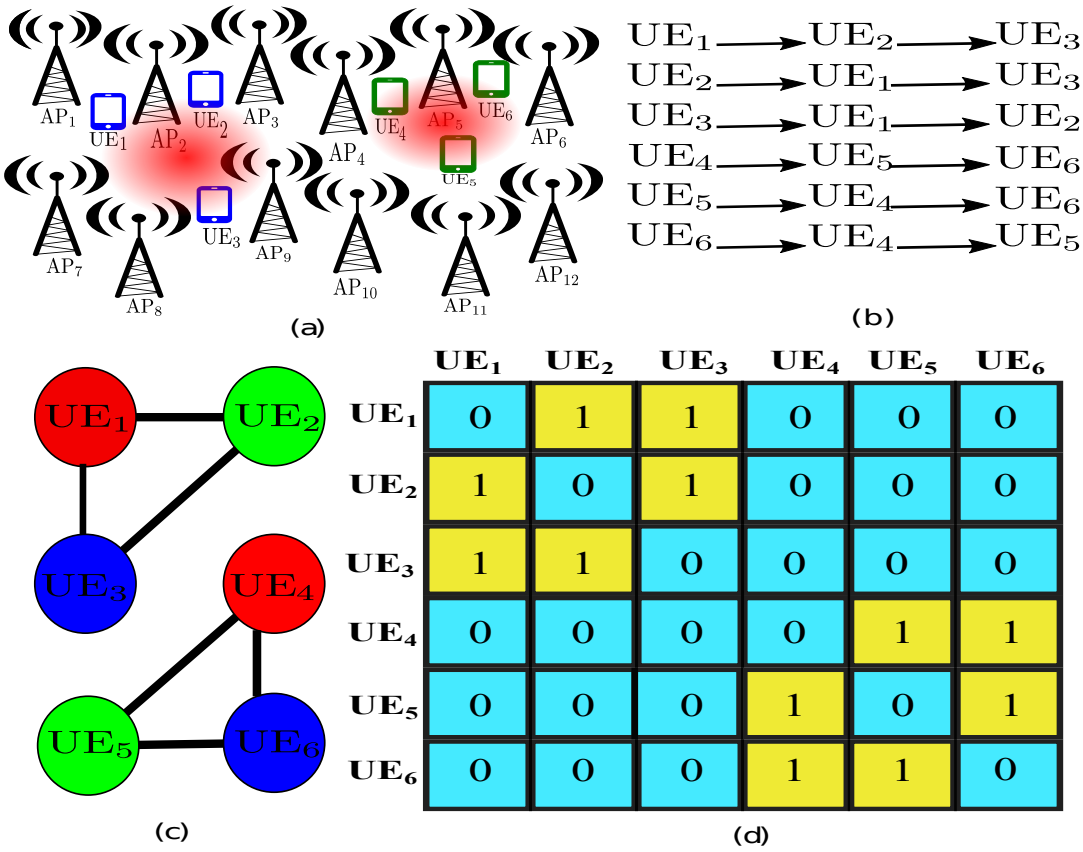

	UE1	UE2	UE3	UE4	UE5	UE6
UE1	0	1	1	0	0	0
UE2	1	0	1	0	0	0
UE3	1	1	0	0	0	0
UE4	0	0	0	0	1	1
UE5	0	0	0	1	0	1
UE6	0	0	0	1	1	0

Figure 4.1: (a) Random pilot reuse: each UE is randomly assigned a pilot sequence from a set of orthogonal sequences. It is to mention that the UEs colored with the same color, share the same DL pilot. This may cause a severe interference between the UEs, e.g., UEs in the red shadow zone. (b) Adjacency list. (c) Conflict graph of the proposed scheme: 3 pilots are used for 6 UEs alleviating the pilot contamination. (d) Adjacency matrix: each of the 1's in the adjacency matrix is equivalent to an edge in the conflict graph.

Based on λ_{th}, we generate an adjacency matrix $A = [\alpha_{kk'}]_{K\times K}$ whose entries are defined as follows

$$\alpha_{kk'} = \begin{cases} 1, & \text{if } \theta_{kk'} > \lambda_{\text{th}}, \\ 0, & \text{otherwise.} \end{cases} \tag{4.2}$$

As Θ, A is symmetric. Later, the adjacency matrix is used to construct the adjacency list and then the conflict or interference graph is used to describe the interference relationship among all UEs in the cell-free massive MIMO system. To bring the image closer to the eye, we exemplified the problem in Figure 4.1. We consider a system involving 6 UEs, i.e., $K = 6$. Based on Θ of this case, we create an adjacency list of this system represented in

Figure 4.1(b). Let's describe the first line in the adjacency list as follows. UE_1 is in conflict with UE_2 and UE_3 that means that the $\theta_{1,2}$ and $\theta_{1,3}$ are superior to a predefined threshold λ_{th}. Similarly, the same process is applied for the other lines in the adjacency list. Then, a conflict graph is constructed in Figure 4.1(c) to describe the relationship between UEs in this example. Every edge of the conflict graph represents a conflict between two vertices (UEs) and distinct vertex colors represent distinct (orthogonal) pilots. An adjacency matrix A of this example is illustrated in Figure 4.1(d).

4.2.2 The proposed algorithm

Using a graph theoretic approach, the problem of pilot allocation consists in coloring the conflict graph according to these rules: (i) vertices that are joined by an edge are given different colors, i.e., once two UEs are in conflict, we should avoid assigning the same pilot to them; and (ii) the number of colors being used is minimized. Hence, mathematically, the optimization problem of vertex coloring can be formulated as follows

$$\min K_{\text{tr}}, \quad \text{s.t.} \quad c_k \neq c_{k'}, \quad \text{if } \alpha_{kk'} = 1, \tag{4.3}$$

where K_{tr} is the required number of colors (training resources) to color the graph and c_k is the color assigned to the k-th UE where $k \in \{1, 2, \ldots, K\}$. We notice that only K DL pilots are available and there is no restriction for the number of times a pilot (color) can be reused. We conjecture that the problem in (4.3) is NP-hard leading to prohibitive complexity. As a consequence, we need to turn around heuristic and suboptimal algorithm to solve this problem. For further details, three constructive algorithms for the graph coloring problem, namely the GREEDY, DSATUR, and RLF algorithms are found in this book [63].

In our work, we use a greedy algorithm to solve the graph coloring problem sequentially. In every step, the greedy algorithm makes certain choices. Its principle is to choose the solution that seems to be the best one locally without considering the consequences that may occur and without going back.

We propose a Graph Coloring based Pilot Assignment in Cell-Free massive MIMO (GC-PA-CF-mMIMO) in **Algorithm 1**, whose physical meaning can be explained step by step as follows:

As an input, we consider the system parameters (K, M, $\{\beta_{mk}\}$, and λ_{th}), and we assign the same DL pilot to all UEs.

Algorithm 1: Proposed GC-PA-CF-mMIMO scheme

Input: System parameters: K, M, $\{\beta_{mk}\}$, and λ_{th};
Assigning the same DL pilot to all UEs.
Output: Colored vertices, i.e., pilots assigned to all UEs.
Step 1: Construction of conflict graph based on $R_k^{\text{iCSI,CF}},\ k = 1, \ldots, K$.
Step 2: Sorting the vertex set $\{\text{UE}_1, \ldots, \text{UE}_K\}$ in descending order with respect of $d_k,\ k = 1, \ldots, K$.
Step 3: Assign the vertex with the highest degree the color $c_1 = 1$.
Step 4:
for $i,\ 2 \leqslant i \leqslant K$ **do**
if $\mathcal{NC}_i = \{1, 2, \ldots, K_{i-1}\}$ **then**
assign a new color, $c_i = K_i$;
else
$c_i = k$ with k satisfying (4.6).
end for

1. **Step 1:** We construct the conflict graph by using $R_k^{\text{iCSI,CF}}$ and the adjacency matrix A.

2. **Step 2:** We sort the vertex set $\{\text{UE}_1, \ldots, \text{UE}_K\}$ in a descending manner according to the degree of the k-th vertex UE_k given as:

$$d_k = \sum_{k'=1}^{K} \alpha_{kk'}, \quad k = 1, \ldots, K, \tag{4.4}$$

   i.e., the number of edges incident to the vertex UE_k, $k = 1, \ldots, K$. In other terms, d_k presents the number of UEs in conflict with the vertex UE_k. The resulting sorted set of step 2 is denoted by V_{sorted}. In the following steps, we introduce V_i as an i-indexed vertex of the V_{sorted} to color, K_i is the number of colors used after assignment of colors to the first i vertices and c_i is the color used for V_i, $\forall\, 1 \leqslant i \leqslant K$.

3. **Step 3**: In this step, firstly, we focus on coloring V_1 assigning any color to it. By convention, the first color assigned is coded by number one, i.e., $c_1 = 1$. More generally, each new color is incremented by one compared to the previous color used as it will be faced in case 1 in step 4. Once the coloring of V_1 is performed, we fix the number of colors in step 3 to $K_1 = 1$.

4. **Step 4 (loop for):** For each loop iteration i, $\forall i \geq 2$, we color V_i. To this end, we have to take into consideration the previously colored vertices indexed by the index

set $\mathcal{I}_i^{\text{c}} = \{1, 2, \ldots, i-1\}$. The coloring of each vertex V_i must respect the following rule to avoid conflict between vertices V_i and V_k,

$$c_i \neq c_k, \quad \text{if } \alpha_{ik} = 1, \quad \forall\, k \in \mathcal{I}_i^{\text{c}}. \tag{4.5}$$

We consider $\mathcal{NC}_i$ the set of all colors assigned to vertices in $\mathcal{I}_i^{\text{c}}$, which are neighbors with vertex V_i. To color the latter, two cases arise:

- **Case 1 (line 2):** If $\mathcal{NC}_i = \{1, 2, \ldots, K_{i-1}\}$, i.e., all previously used colors appear on vertices neighbors with vertex V_i, then we assign a new color to vertex V_i denoted $c_i = K_i$ where $K_i = K_{i-1} + 1$.
- **Case 2 (line 3)**: If the authorized color set to color the vertex V_i, denoted $\mathcal{AC}_i = \{1, 2, \ldots, K_{i-1}\} - \mathcal{NC}_i$, is non-empty, then to color vertex V_i we reuse a color k, i.e. $c_i = k$,

  $$k = \arg \min_{j \in \mathcal{AC}_i} n_j \tag{4.6}$$

  where n_j is the number of vertices indexed in $\mathcal{I}_i^{\text{c}}$ that have been colored by color j. In other terms, k is the lowest numbered color that has not been used on any previously colored vertices neighbors with V_i. Thus, $K_i = K_{i-1} < i$. In that case, we prevent excess use of colors (pilots) as we reuse colors.

4.2.3 Threshold method selection

The threshold value λ_{th} is applied to determine whether UEs are in conflict or not. If we have $\theta_{k,k'} > \lambda_{\text{th}}$, UE_k and $\text{UE}_{k'}$ are in conflict so that they can't reuse the same pilot. If we have $\theta_{k,k'} \leq \lambda_{\text{th}}$, UE_k and $\text{UE}_{k'}$ are not in conflict so that they can reuse the same pilot. Let's consider the minimum and the maximum of $\theta_{k,k'}$, i.e. $\theta_{\text{min}} = \min\{\theta_{k,k'}\}$, $\theta_{\text{max}} = \max\{\theta_{k,k'}\}$. According to the value of λ_{th} chosen, we have different conflict graphs. From (4.2), it is obvious that $\forall \lambda_{\text{th}} \in]-\infty, \theta_{\text{min}}]$. Therefore, the lower limit of λ_{th} is θ_{min}. As well, the upper limit of λ_{th} is θ_{max}. Thus, $\lambda_{\text{th}} \in [\theta_{\text{min}}, \theta_{\text{max}}]$.

Let's consider the two following extreme cases. When the threshold λ_{th} is fixed to θ_{max}, there is no conflict between UEs. When we decrease the threshold λ_{th}, this leads to potential conflict between UEs. Thus, the algorithm GC-PA-CF-mMIMO can mitigate the interference with a decreased number of DL pilots (colors). When the threshold λ_{th} is fixed to θ_{min}, the conflict appears among all UEs and the number of DL pilots (colors) required

is K pilots. The algorithm GC-PA-CF-mMIMO in this case is assimilated to an orthogonal pilot allocation scheme.

As in [24], in order to determine the near-optimal threshold λ_{th}, we propose an algorithm called iterative grid search (IGS) as

$$\lambda_{\text{th}} = f_{\text{IGS}}([\theta_{\text{min}}, \theta_{\text{max}}], N, T), \tag{4.7}$$

where T represents the number of iterations and N denotes the number of grids per iteration. In short, it consists in selecting the threshold λ_{th} from N grids that maximizes the minimum per-user DL net throughput in every iteration until it reaches T iterations. The description of the algorithm per iteration is as follows:

- Iteration 1: Let's consider the N threshold grids for the first iteration by the grid set $\mathcal{G} = \{\lambda_i^{(1)} : 1 \leqslant i \leqslant N\}$, $\lambda_0^{(1)} = \theta_{\text{min}}$, $\lambda_{i+1}^{(1)} = \lambda_i^{(1)} + \Delta^{(1)}$ and $\Delta^{(1)} = \frac{\theta_{\text{max}} - \theta_{\text{min}}}{N-1}$. We denote $\lambda_{\text{max}}^{(1)}$ the grid element from the grid set $\mathcal{G}$ that can reach the maximum of the minimum per-user DL net throughput. A sub-interval 1 denoted as follows $[\lambda_{\text{max}}^{(1)} - \Delta^{(1)}/2, \lambda_{\text{max}}^{(1)} + \Delta^{(1)}/2]$. It will be used for the next iteration as a search interval of $\lambda_{\text{max}}^{(2)}$.

- Iteration t, $2 \leqslant t \leqslant T$: Once we find the $\lambda_{\text{max}}^{(t)}$, we narrow the search sub-interval t and we get the interval search $[\lambda_{\text{max}}^{(t)} - \Delta^{(t)}/2, \lambda_{\text{max}}^{(t)} + \Delta^{(t)}/2]$. This step is performed for $(T-1)$ times. Finally, the near-optimal threshold is $\lambda_{\text{th}} = \lambda_{\text{max}}^{(T)}$.

4.3 Numerical results and discussion

This section presents a quantitative study to assess the performance, in terms of per-user downlink net throughput, of our proposed solution and the existing solutions in the litterature. The M APs and K UEs are uniformly and randomly distributed within a square of size 1 km^2. To simulate a cell-free topology, i.e., to avoid cell-edge effects, the square simulation area is wrapped around with eight clones of neighbor squares to deal with a network with infinite area (wrap-around technique).

4.3.1 Large-scale fading model

Considering the model used in (3.3), we emphasize on the large-scale fading coefficient β_{mk}, which modelizes the path-loss and the shadow fading as follows

$$\beta_{mk} = \mathrm{PL}_{mk}.10^{\frac{\sigma_{\mathrm{sh}} z_{mk}}{10}}, \tag{4.8}$$

where PL_{mk} represents the path loss and $10^{\frac{\sigma_{\mathrm{sh}} z_{mk}}{10}}$ represents the shadow fading with the standard deviation σ_{sh}, and $z_{mk} \sim \mathcal{CN}(0,1)$, i.e., we assume uncorrelated shadow-fading.

4.3.1.1 Path-loss model

We use three-slope model to model the path-loss [8, 14]. Three values of loss exponent can be distinguished according to the distance between the k-th UE and the m-th AP, denoted by d_{mk}. More particularly, the path-loss exponent is equal to 3.5 if $d_{mk} > d_1$, to 2 if $d_0 < d_{mk} \leq d_1$, and to 0 if $d_{mk} \leq d_0$. We use *Hata-COST231* [64] as a propagation model for path-loss PL_{mk} (in dB) as follows

$$\mathrm{PL}_{mk} = \begin{cases} -L - 35\log_{10}(d_{mk}), & \text{if } d_{mk} > d_1, \\ -L - 15\log_{10}(d_1) - 20\log_{10}(d_{mk}), & \\ \qquad\qquad \text{if } d_0 < d_{mk} \leq d_1, & \\ -L - 15\log_{10}(d_1) - 20\log_{10}(d_0), \text{if } d_{mk} \leq d_0, & \end{cases} \tag{4.9}$$

where

$$\begin{aligned} L = \quad & 46.3 + 33.9\log_{10}(f) - (1.1\log_{10}(f) - 0.7)h_{\mathrm{UE}} \\ & - 13.82\log_{10}(h_{\mathrm{AP}}) + (1.56\log_{10}(f) - 0.8), \end{aligned} \tag{4.10}$$

and where f is the carrier frequency (in MHz), h_{AP} (in m) is the height of the AP and h_{UE} (in m) is the height of the UE antenna. We shall mention that when $d_{mk} \leq d_1$, there is no shadowing, i.e., the transmitters/receivers are not surrounded by common obstacles.

4.3.2 Orthogonal training matrix selection

The orthogonal training matrix used both in UL and DL is constructed from a discrete Fourier matrix [2, 65, 66] as follows:

1. Choose the entries of discrete Fourier matrix W that can be denoted as $W = \left(\frac{\omega_L^{(j-1)(j'-1)}}{\sqrt{L}}\right)_{j,j'=1,\ldots,L}$,

where $L = \tau_{\text{ul,p}} = \tau_{\text{dl,p}} = K$ for orthogonal pilot assignment in UL and DL training equivalently:

$$W = \frac{1}{\sqrt{L}} \begin{bmatrix} 1 & 1 & 1 & 1 & \cdots & 1 \\ 1 & \omega_L & \omega_L^2 & \omega_L^3 & \cdots & \omega_L^{L-1} \\ 1 & \omega_L^2 & \omega_L^4 & \omega_L^6 & \cdots & \omega_L^{2(L-1)} \\ 1 & \omega_L^3 & \omega_L^6 & \omega_L^9 & \cdots & \omega_L^{3(L-1)} \\ \vdots & \vdots & \vdots & \vdots & \ddots & \vdots \\ 1 & \omega_L^{L-1} & \omega_L^{2(L-1)} & \omega_L^{3(L-1)} & \cdots & \omega_L^{(L-1)(L-1)} \end{bmatrix}$$

where $\omega_L = e^{-2\pi i/L}$ is a primitive L-th root of unity in which $i^2 = -1$. We notice that these matrix entries are located at L different equally spaced points on the unit circle. Then, they correspond to a L-ary phase-shift keying (PSK) constellation.

2. Design of the training matrix of size, respectively, equal to $K \times \tau_{\text{ul,p}}$ in UL and equal to $K \times \tau_{\text{dl,p}}$ in DL, by a random permutation of K row vectors.

4.3.3 Parameters and setup

In all examples, all simulation parameters are summarized in Table 4.1 [8, 14]. The parameters $(\overline{\rho}_{\text{ul,p}}, \overline{\rho}_{\text{ul,d}}, \overline{\rho}_{\text{dl,p}}, \overline{\rho}_{\text{dl,d}})$ are, respectively, the transmit powers of UL pilot, UL data, DL pilot and DL data. The corresponding normalized SNRs $(\rho_{\text{ul,p}}, \rho_{\text{ul,d}}, \rho_{\text{dl,p}}, \rho_{\text{dl,d}})$, defined in Section 3.4, are computed by dividing the aforementioned radiated powers by the noise power, whose formula is given by

$$\text{noise power} = B \times k_{\text{B}} \times T_0 \times \text{noise figure (W)}, \tag{4.11}$$

where B is the spectral bandwidth (Hz), $k_{\text{B}} = 1.381 \times 10^{-23}$ (Joule per Kelvin) is the Boltzmann constant, and $T_0 = 290$ (Kelvin) is the noise temperature. We choose the noise figure (in UL and DL) equal to 9 dB and $\tau_{\text{c}} = 200$ symbols, corresponding to a coherence bandwidth $B_{\text{c}} = 200$ kHz and a coherence time $T_{\text{c}} = 1$ ms. In what follows B is fixed at 20 MHz and the antenna gain at 0 dBi. In our simulation, we suppose that $K \ll \tau_{\text{c}}$ and $\tau_{\text{ul,p}}\tau_{\text{dl,p}} \geq K$. Added to that, the channel estimation in UL and DL occur at the same coherence time.

We define the DL per-user net throughput [5] T_k (bit/s), which is proportional to the

Table 4.1: Simulation parameters

Description	Value	Description	Value
APs/UEs	unif. rand. dist	h_{UE}	1.65 m
τ_{c}	200 symbols	h_{AP}	5 m
simulation area	1 km^2	coherence time	1 ms
path-loss model	three-slope	d_0, d_1	10, 50 m
carrier frequency f	2 GHz	noise figure	9 dB
shadow-fading	uncorrelated	$\overline{\rho}_{\text{dl,d}}$, $\overline{\rho}_{\text{dl,p}}$	200 mW
shadow-fading std	8 dB	$\overline{\rho}_{\text{ul,d}}$, $\overline{\rho}_{\text{ul,p}}$	100 mW
bandwidth B	20 MHz	antenna gain	0 dBi

DL per-user rate R_k (bit/s/Hz), as follows

$$T_k = B\xi^{\text{DL}}(1 - \frac{\tau_{\text{po}}}{\tau_{\text{c}}})R_k, \tag{4.12}$$

where B is the spectral bandwidth and τ_{po} is the pilot overhead, i.e., the number of samples per coherence interval spent in uplink and downlink training phase. On the one hand, T_k takes into consideration only the fraction of samples in each coherence interval that are dedicated for transmission of payload data $(1 - \frac{\tau_{\text{po}}}{\tau_{\text{c}}})$, i.e., we subtract the resources for UL and DL pilots transmission. On the other hand, to get both UL and DL spectral efficiencies simultaneously, the net spectral efficiencies must be multiplied also by a factor ξ^{DL} to allocate the fraction of useful samples per coherence interval that are used for DL. For instance, for a symmetric TDD frame ($\tau_{\text{ul,d}} = \tau_{\text{dl,d}}$), i.e., $\xi^{\text{DL}} = \frac{1}{2}$, the per-user throughput is $T_k = \frac{B}{2}(1 - \frac{\tau_{\text{po}}}{\tau_{\text{c}}})R_k$.

4.3.4 Results and discussion

In what follows, we deal with an example to show the advantage of our proposed solution compared to the state-of-the-art. On the one hand, for uplink pilot allocation, we used only orthogonal pilot assignment. On the other hand, for DL pilot allocation, our study is based on the following methods:

1. ***Statistical CSI (sCSI)***: No DL training is conducted and all the UEs use the sCSI to decode its intended data. We allocate to each UE an orthogonal UL pilot. So, $\tau_{\text{ul,p}} = K, \tau_{\text{dl,p}} = 0$;

2. ***Instantaneous CSI (iCSI) with orthogonal DL pilots***: The DL training is conducted

for all UEs. We allocate to each UE an orthogonal UL pilot and each UE receives an orthogonal DL pilot to estimate the DL channel. Hence, $\tau_{\text{ul,p}} = \tau_{\text{dl,p}} = K$;

3. ***Instantaneous CSI (iCSI) with DL random pilot assignment***: The DL training is performed for all UEs. We allocate to each UE an orthogonal UL pilot and each UE receives a DL pilot randomly from a set of orthogonal sequences with a length pilot sequence $\tau_{\text{dl,p}}^{\text{rand}}$. In order to work in same conditions for random pilot assignment and coloring pilot assignment defined by a length pilot sequence $\tau_{\text{dl,p}}^{\text{color}}$, we fix $\tau_{\text{dl,p}}^{\text{rand}} = \tau_{\text{dl,p}}^{\text{color}}$. For the random pilot assignment, two UEs may receive the same pilot randomly;

4. ***Instantaneous CSI (iCSI) with coloring pilot assignment(proposed scheme)***: The DL training is performed for all UEs. We allocate to each UE an orthogonal UL pilot and each UE receives a DL pilot following the coloring algorithm GC-PA-CF-mMIMO. Especially the UEs between which we have $\theta_{k,k'}$ respecting $\theta_{k,k'} < \lambda_{\text{th}}$, can reuse the same pilot. On the contrary, the UEs between which we have $\theta_{k,k'}$ respecting $\theta_{k,k'} \geq \lambda_{\text{th}}$, don't reuse the same pilot otherwise it will cause more and more interference between UEs.

Moreover, to fix the power control coefficients η_{mk} at the m-th AP for the k-th UE, we implement a simple equal (uniform) power control policy with

$$\eta_{mk} = (\sum_{k'=1}^{K} \gamma_{mk'})^{-1} \; \forall k = 1, \ldots, K, m = 1, \ldots, M, \tag{4.13}$$

satisfying the equality condition in (3.11), i.e., each AP uses full power. This technique, denoted by channel-dependent full power transmission (CD-FPT), is not optimal but it can be performed in a distributive way, and it reduces the complexity of computation as it doesn't take into consideration an optimization problem.

Figure 4.2(a) and Figure 4.2(b) exemplify, respectively, for two channel setups, the IGS algorithm to determine the near-optimal threshold λ_{th} with $M = 60$, $K = 10$, $N = 20$, and $T = 1$. The X-axis represents the normalized threshold interval, and the Y-axis represents the min-user DL net throughput of the proposed GC-PA-CF-mMIMO considering the threshold grid set per iteration t $\{\lambda_i^{(t)} : 1 \leqslant i \leqslant N\}$. As we are limited to $T = 1$, the near-optimal threshold $\lambda_{\text{th}} = \lambda_{\text{max}}^{(1)}$ can be obtained once the first iteration is performed, considering the maximum of the min-user DL net throughput of the proposed GC-PA-CF-mMIMO. We underline that the selection of λ_{th} has an impact on the min-user DL net throughput of

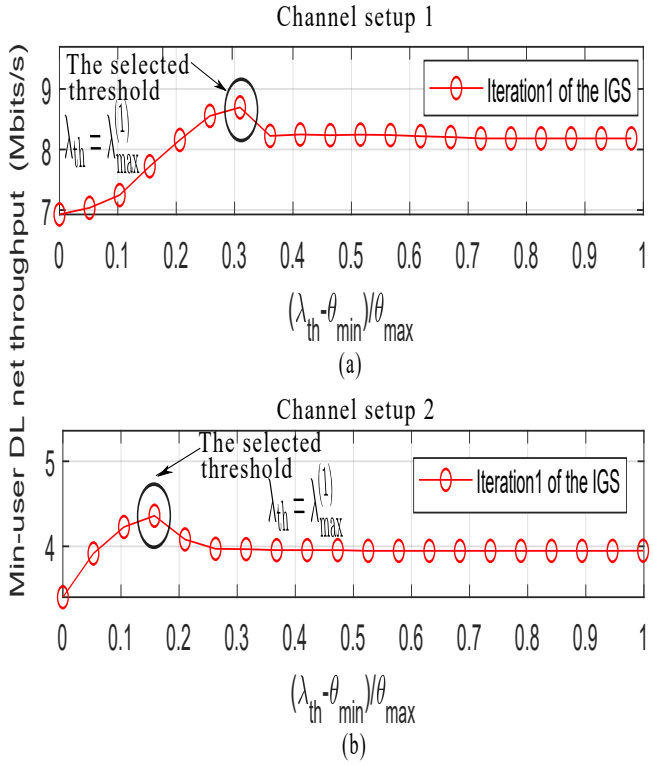

Figure 4.2: The IGS algorithm to determine the near-optimal threshold λ_{th} with $M = 60$, $K = 10$, $N = 20$, and $T = 1$.

the proposed GC-PA-CF-mMIMO. We consider two cases as follows. In case 1, when λ_{th} is equal to θ_{min}, the proposed scheme is assimilated to an orthogonal pilot assignment scheme. In that scheme, K orthogonal pilots are needed. In case 2, when $\lambda_{\text{th}} = \lambda_{\text{max}}^{(1)}$, we reuse pilots using the minimum number of DL pilots and reducing the effect of DL pilot contamination in DL pilot assignment as (4.3) reveals. On the one hand, as a consequence, the pilot sequence length decreases compared to case 1. This increases the min-user DL net throughput. On the other hand, the reduction in pilot sequence length comes at the expense of the increase of the number of identical pilot sequences, hence, the increase in the DL channel estimation error quality, which decreases the min-user DL net throughput. Thus, there is a tradeoff on the pilot sequence length depending on the considered channel setup.

The gain yield by the proposed scheme in terms of min-user DL net throughput is shown in Figure 4.3 with $M = 60$, $K = 10$. The curves related to the scheme sCSI and the random pilot assignment are almost superimposable. We underline that the DL orthogonal

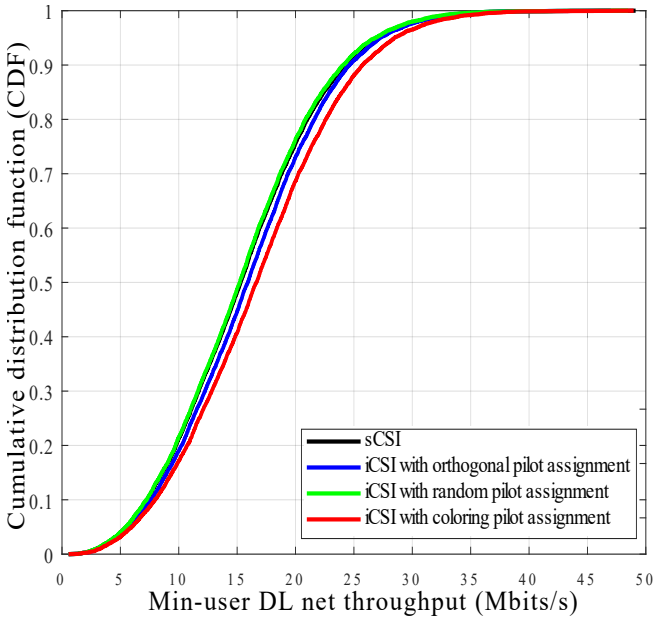

Figure 4.3: The CDF of min-user DL net throughput with $M = 60$, $K = 10$.

pilot assignment outperforms the DL random pilot assignment by about 0.27 Mbits/s in concordance with the UL case in [21], and another gain of about 0.83 Mbits/s can be achieved by the proposed coloring algorithm as it eliminates the potential IUI using the graph conflict and it reduces the number of DL pilots. The proposed scheme outperforms the DL random pilot assignment. The latter strategy doesn't take into consideration the conflict between UEs, so that those in close vicinity may reuse the same DL pilot, which increases DL pilot contamination. The DL orthogonal pilot assignment outperforms the scheme sCSI. As cell-free massive MIMO is characterized by a channel hardening not sufficiently pronounced, UEs rely on beamformed DL pilots to estimate DL channel with more accuracy [15].

Figure 4.4 represents the average min-user DL net throughput against M with $K = 10$. The performance of prior art and the proposed scheme increase continually when M increases thanks to the diversity gain. Especially, whatever the value of M, the proposed scheme outperforms the prior art mentioned before by about 1 Mbits/s.

Figure 4.5 represents the average DL pilot overhead ratio defined by,

$$\text{DL pilot overhead ratio} = \frac{\tau_{\text{dl,p}}^{\text{color}}}{\tau_{\text{dl,p}}^{\text{orth}}}, \tag{4.14}$$

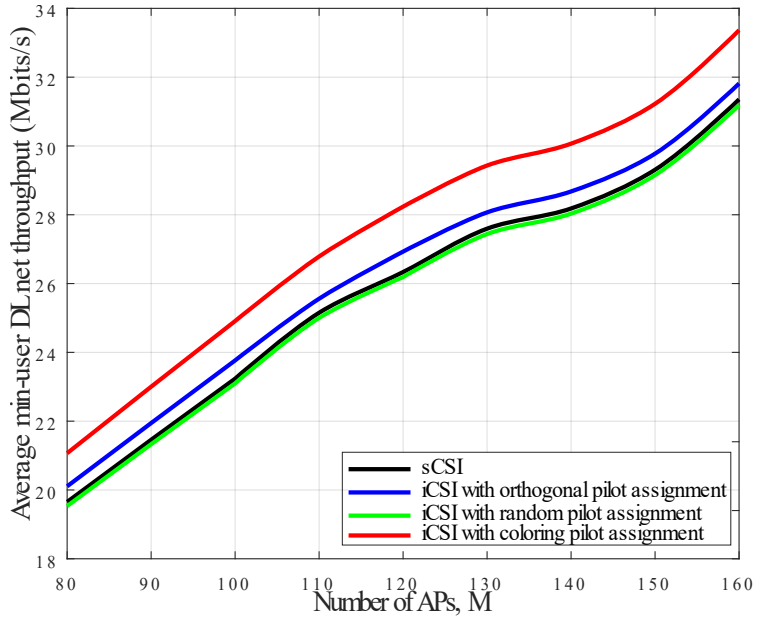

Figure 4.4: The average min-user DL net throughput versus the number of APs. Here $K = 10$.

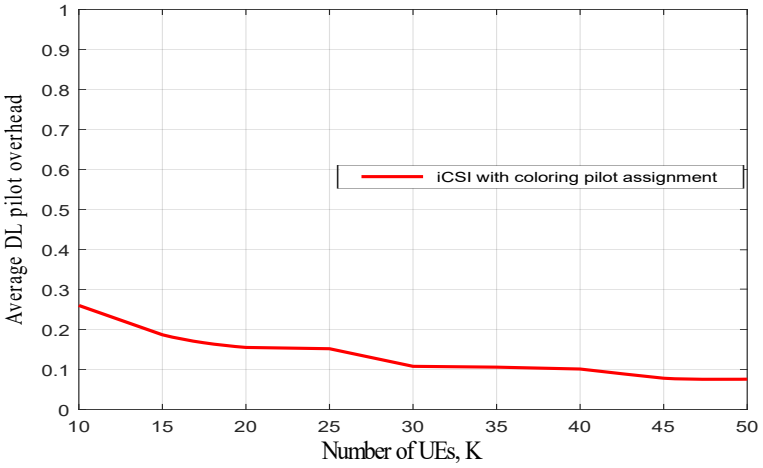

Figure 4.5: The average DL overhead ratio versus the number of UEs. Here, $M = 60$.

versus the number of UEs K when $M = 60$. In other terms, the DL pilot overhead ratio computes the DL pilot size reduction using the proposed scheme in comparison to the orthogonal DL pilot assignment scheme. It is to notice that the number of orthogonal pilots using the orthogonal pilot assignment is equal to the number of UEs, K. Furthermore, we highlight that the average DL overhead ratio for the proposed scheme is smaller than the

one for the orthogonal pilot assignment, as in the proposed scheme we reuse DL pilots so that we reach the minimum of DL pilot size as (4.3) reveals. Added to that, the DL overhead ratio for the proposed scheme is inversely proportional to the number of UEs. For the proposed scheme, when K varies between 10 to 30, the DL pilot overhead ratio varies between 0.25 to 0.1, and when K varies between 30 to 50, the DL pilot overhead ratio is almost constant and equal to 0.1. The more we have UEs to serve, the more DL beamformed pilots are needed to mitigate the DL pilot contamination.

4.4 Conclusion

Throughout this chapter, qualitatively, we proposed a graph coloring algorithm to reduce the DL pilot overhead while considering the DL pilot contamination issue. It consists on studying under which conditions the UEs are likely to have a severe interference induced by one UE to another one. Consequently, based on that we designed a conflict graph in which a vertex denotes a UE and the edge between the vertices denote that the UEs are in conflict. Based on an optimization problem to color the vertices, i.e. assign pilots to UEs, we used a coloring algorithm. In consequence, we reduced the number of DL pilots taking into account the DL pilot contamination problem. Quantitatively, we proved that the DL pilot assignment based on our proposed algorithm outperforms, in terms of min-user DL net throughput, some prior works such as the DL orthogonal pilot assignment and the DL random pilot assignment.

Chapter 5

Conclusion and perspectives

> “ The important thing is not to stop questioning. Curiosity has its own reason for existing.
>
> *Albert Einstein* ”

In this manuscript, in response to the aforementioned problematic, we presented thoroughly our main contributions. In the first section of this final chapter, we summarize our contributions, and we introduce our future research directions in Section 5.2.

5.1 Summary of contributions

In this thesis, in chapter 2, we presented the purposes of using a massive number of antennas in cellular networks. Specifically, it enhances the spectral efficiency and improves energy efficiency using simple linear processing rather than advanced signal processing thanks to the favorable propagation. More precisely, even with a simple maximum-ratio combining (MRC) in the UL or maximum-ratio transmission (MRT) in the DL, the effects of fast fading, intracell interference, and uncorrelated noise tend to disappear as the number of BS station antennas grows large. Moreover, it diminishes the latency thanks to the beamforming, via numerous antennas in line with the law of large numbers, especially for UEs which are hard to reach with a good signal. Besides, throughout the channel estimation, the CSI is negatively impacted by the use of non-orthogonal pilots, causing a "pilot contamination problem". In chapter 3, we studied the paradigm shift from conventional massive MIMO in cellular network to massive MIMO in cell-free networks. The reason for such a shift is mainly to offer better performance to cell-edge UEs in massive MIMO in cellular networks.

Furthermore, the main advantage of opting for cell-free massive MIMO is the spatial multiplexing, as each UE receives the same signal transmitted from APs situated in different sites by using channels with different characteristics. Besides, the channel hardening in cell-free massive MIMO is less accentuated compared to cellular massive MIMO. So, the UEs, having low degree of channel hardening, rely on iCSI based on beamformed DL pilots.

As contributions of our work, in chapter 4, we proposed a graph coloring based approach to reduce DL pilot contamination and to decrease the DL pilot overhead due to the DL pilot utilization required for DL channel estimation in the context of cell-free massive MIMO system. It is conducted by relaxing the orthogonality property of DL pilots, which generates the DL pilot contamination effect. First, considering this effect, we selected an appropriate threshold. Then, in order to model the potential interference relationship among all UEs, we designed an interference or conflict graph. After that, an algorithm GC-PA-CF-mMIMO is proposed to assign DL pilots to the UEs, eliminating the predominant interference dealt in the conflict graph. Precisely, this algorithm allows to reuse DL pilots, making them fewer, and therefore, reducing their size, in combination with mitigating DL pilot contamination. Consequently, using the proposed algorithm, in cell-free massive MIMO, the gain in terms of min-user DL net throughput is increased compared to the conventional pilot assignment techniques in cell-free massive MIMO [8, 21]. We notice that the DL pilot overhead ratio, using the proposed scheme, is reduced compared to the DL orthogonal pilot assignment.

5.2 Perspectives

Cell-free massive MIMO is an emerging topic, which still presents many challenges. It leads to a wide spectrum of future directions. Our study can be extended to search for a more efficient method to select the threshold than the one that we adopted in this thesis, iterative grid search, as it represents a sub-optimal solution. Then, selecting a more accurate threshold leads us to generate a more adapted conflict graph, then, the DL pilot contamination is decreased more and more. Added to that, in case the number of pilots is limited, in response to prioritizing UEs in accordance with their channel conditions, i.e., assigning pilots to certain UEs is considered more important than others, a *weighted graph coloring* can be adopted [67]. Besides, relying on the channel hardening degree and the mobility of a UE, some UEs may not require that the APs beamform DL pilots to them as it was revealed in [14]. That's why a resort to using a graph coloring DL pilot assignment [68] within the

group of UEs that require DL pilots may be an efficient alternative. Added to that, it is interesting to study if it is possible that UEs rely on blind channel estimation to estimate the DL channel, i.e., using the data symbols, without having recourse to beamformed DL pilots in cell-free massive MIMO. Some areas require invisible installations of communication systems. In this regard, it may be convenient to study the performance of the spectral efficiency in cell-free massive MIMO with the radio stripe architecture not only in UL as [69] but also in DL.

The recent studies in cell-free massive MIMO were performed using Rayleigh fading channels. It is interesting to study the potential performance of cell-free massive MIMO considering practical channels combining LoS and non-LoS paths depending on the carrier frequency. Furthermore, another key is to investigate new power control policies in a distributed fashion and with a scalable implementation.

Another emerging systems that can be explored are the *large intelligent surfaces (LIS)* [70], which enable not only communication but also more applications such as remote sensing and positioning. These active surfaces generate and transmit its own signals to the UEs. These active surfaces don't enhance an existing communication, replacing the BSs, enable communication with UEs in near field, i.e. channels mostly line of sight, while in massive MIMO systems UEs are in far fields. It can be some improvements to reduce the redundancy in terms of computational requirements within the panels in LIS [71]. This problem may be improved using a coloring graph. Added to that, it has been a recent interest in reflective/passive surfaces called *reconfigurable intelligent surfaces (RIS)* [72, 73], which mimic what a mirror does but in a controllable way. So that it represents an additional channel path, similar to a relay to control how the channel behaves [74]. Control interfaces, which require a control interface, includes a communication link to a BS and internal control of the individual reflecting elements. These interface surfaces are implemented to control the intelligent surfaces including channel estimation via training pilots to estimate the location of the UE and so that the intelligent surfaces focus the signal towards the intended UE. Massive MIMO is no longer a promising concept for wireless networks, in 2018 it was deployed in some countries. What's next to that? The cutting-edge researchs include neural networks in massive MIMO [75] and other inspiring and challenging issues such as intelligent massive MIMO (RIS and LIS), holographic massive MIMO and extremely large aperture arrays, summarized in [76–78].

Appendices

Appendix A

Publications of the thesis

1. W. H. Hmida, V. Meghdadi, A. Bouallegue, J. P. Cances, "Graph Coloring Based Pilot Reuse Among Interfering Users in Cell-Free Massive MIMO", in *Proc.* IEEE Int. Conf. Commun. (ICC), Jun 2020, Dublin, Irlande.
2. W. H. Hmida, V. Meghdadi, A. Bouallegue, J. P. Cances, "Graph Coloring Based Pilot Assignment to Mitigate Downlink Pilot Contamination for Cell-Free Massive MIMO Systems". Submitted to IET communications.

Appendix B

Proof of equations

B.1 Proof of equation 3.6

Assuming a prior information $\tilde{y}_{\mathrm{ul,p},mk}$ as follows

$$\tilde{y}_{\mathrm{ul,p},mk} = \varphi_k^H \boldsymbol{y}_{\mathrm{ul,p},m} = \sqrt{\tau_{\mathrm{ul,p}}\rho_{\mathrm{ul,p}}} g_{mk} + \varphi_k^H \boldsymbol{w}_{\mathrm{ul,p},m}, \tag{B.1}$$

via the MMSE estimator of g_{mk}. g_{mk} is estimated as follows,

$$\hat{g}_{mk} = \mathbb{E}(g_{mk}|\tilde{y}_{\mathrm{ul,p},mk}); \tag{B.2}$$

$$= \underbrace{\mathbb{E}(g_{mk})}_{(a)} + \underbrace{\mathrm{Cov}(g_{mk}, \tilde{y}_{\mathrm{ul,p},mk})}_{(b)} \underbrace{(\mathrm{Cov}(\tilde{y}_{\mathrm{ul,p},mk}))}_{(c)}^{-1} (\tilde{y}_{\mathrm{ul,p},mk} - \underbrace{\mathbb{E}(\tilde{y}_{\mathrm{ul,p},mk})}_{(d)}). \tag{B.3}$$

Let's describe the terms of $\hat{g}_{mk}$ one by one as follows:

- (a): $\mathbb{E}(g_{mk}) = 0$;
- (b): $\mathrm{Cov}(g_{mk}, \tilde{y}_{\mathrm{ul,p},mk}) = \mathbb{E}((g_{mk} - \mathbb{E}(g_{mk}))(\tilde{y}_{\mathrm{ul,p},mk} - \mathbb{E}(\tilde{y}_{\mathrm{ul,p},mk}))^{\mathrm{H}}) = \mathbb{E}(g_{mk}(\tilde{y}_{\mathrm{ul,p},mk})^{\mathrm{H}})$;
  $= \mathbb{E}(\sqrt{\tau_{\mathrm{ul,p}}\rho_{\mathrm{ul,p}}} g_{mk}^2) = \sqrt{\tau_{\mathrm{ul,p}}\rho_{\mathrm{ul,p}}}\beta_{mk}$
- (c): $\mathrm{Cov}(\tilde{y}_{\mathrm{ul,p},mk}) = \mathbb{E}(\tilde{y}_{\mathrm{ul,p},mk} - \mathbb{E}(\tilde{y}_{\mathrm{ul,p},mk}))(\tilde{y}_{\mathrm{ul,p},mk} - \mathbb{E}(\tilde{y}_{\mathrm{ul,p},mk})^{\mathrm{H}}) = \mathbb{E}(\tilde{y}_{\mathrm{ul,p},mk}(\tilde{y}_{\mathrm{ul,p},mk})^{\mathrm{H}})$;
  $= \mathbb{E}(\sqrt{\tau_{\mathrm{ul,p}}\rho_{\mathrm{ul,p}}} g_{mk} + \varphi_k^H \boldsymbol{w}_{\mathrm{ul,p},m}) \mathbb{E}(\sqrt{\tau_{\mathrm{ul,p}}\rho_{\mathrm{ul,p}}}(g_{mk})^{\mathrm{H}} + \varphi_k(\boldsymbol{w}_{\mathrm{ul,p},m})^{\mathrm{H}})$;
  as $\mathbb{E}(\varphi_k \varphi_k^H) = 1$;
  $\mathrm{Cov}(\tilde{y}_{\mathrm{ul,p},mk}) = \mathbb{E}(\tau_{\mathrm{ul,p}}\rho_{\mathrm{ul,p}} g_{mk}(g_{mk})^{\mathrm{H}}) + \mathbb{E}(\boldsymbol{w}_{\mathrm{ul,p},m}^2) = \tau_{\mathrm{ul,p}}\rho_{\mathrm{ul,p}}\beta_{mk} + 1$
- (d): $\mathbb{E}(\tilde{y}_{\mathrm{ul,p},mk}) = 0$.

As a consequence, $\hat{g}_{mk} = \frac{\sqrt{\tau_{\mathrm{ul,p}}\rho_{\mathrm{ul,p}}}\beta_{mk}}{\tau_{\mathrm{ul,p}}\rho_{\mathrm{ul,p}}\beta_{mk}+1} \tilde{y}_{\mathrm{ul,p},m} = c_{mk}\tilde{y}_{\mathrm{ul,p},m}$, where $c_{mk} \triangleq \frac{\sqrt{\tau_{\mathrm{ul,p}}\rho_{\mathrm{ul,p}}}\beta_{mk}}{\tau_{\mathrm{ul,p}}\rho_{\mathrm{ul,p}}\beta_{mk}+1}$.

B.2 Proof of equation 3.8

$\gamma_{mk} \triangleq \mathbb{E}\left\{|\hat{g}_{mk}|^2\right\} = \mathbb{E}\left\{\left|\frac{\sqrt{\tau_{\mathrm{ul,p}}\rho_{\mathrm{ul,p}}}\beta_{mk}}{\tau_{\mathrm{ul,p}}\rho_{\mathrm{ul,p}}\beta_{mk}+1}\tilde{y}_{\mathrm{ul,p},m}\right|^2\right\}$;
$= \frac{\tau_{\mathrm{ul,p}}\rho_{\mathrm{ul,p}}\beta_{mk}^2}{(\tau_{\mathrm{ul,p}}\rho_{\mathrm{ul,p}}\beta_{mk}+1)^2}\mathbb{E}\left\{|\tilde{y}_{\mathrm{ul,p},m}|^2\right\} = \frac{\tau_{\mathrm{ul,p}}\rho_{\mathrm{ul,p}}\beta_{mk}^2}{(\tau_{\mathrm{ul,p}}\rho_{\mathrm{ul,p}}\beta_{mk}+1)^2}(\tau_{\mathrm{ul,p}}\rho_{\mathrm{ul,p}}\beta_{mk}+1) = \frac{\tau_{\mathrm{ul,p}}\rho_{\mathrm{ul,p}}\beta_{mk}^2}{\tau_{\mathrm{ul,p}}\rho_{\mathrm{ul,p}}\beta_{mk}+1}$;
$= \sqrt{\tau_{\mathrm{ul,p}}\rho_{\mathrm{ul,p}}}\beta_{mk}c_{mk}$.

Bibliography

[1] *IEEE Spectrum [Online]*. Available at https://spectrum.ieee.org/.

[2] Emil Björnson, Jakob Hoydis, Luca Sanguinetti, et al. Massive mimo networks: Spectral, energy, and hardware efficiency. *Foundations and Trends® in Signal Processing*, 11(3-4):154–655, 2017.

[3] Fredrik Rusek, Daniel Persson, Buon Kiong Lau, Erik G Larsson, Thomas L Marzetta, Ove Edfors, and Fredrik Tufvesson. Scaling up mimo: Opportunities and challenges with very large arrays. *IEEE signal processing magazine*, 30(1):40–60, 2012.

[4] Thomas L Marzetta. Noncooperative cellular wireless with unlimited numbers of base station antennas. *IEEE transactions on wireless communications*, 9(11):3590–3600, 2010.

[5] Thomas L Marzetta. *Fundamentals of massive MIMO*. Cambridge University Press, 2016.

[6] Shidong Zhou, Ming Zhao, Xibin Xu, Jing Wang, and Yan Yao. Distributed wireless communication system: a new architecture for future public wireless access. *IEEE Communications Magazine*, 41(3):108–113, 2003.

[7] Hien Quoc Ngo, Alexei Ashikhmin, Hong Yang, Erik G Larsson, and Thomas L Marzetta. Cell-free massive mimo: Uniformly great service for everyone. In *2015 IEEE 16th international workshop on signal processing advances in wireless communications (SPAWC)*, pages 201–205. IEEE, 2015.

[8] Hien Quoc Ngo, Alexei Ashikhmin, Hong Yang, Erik G Larsson, and Thomas L Marzetta. Cell-free massive mimo versus small cells. *IEEE Transactions on Wireless Communications*, 16(3):1834–1850, 2017.

[9] Elina Nayebi, Alexei Ashikhmin, Thomas L Marzetta, and Hong Yang. Cell-free massive mimo systems. In *2015 49th Asilomar Conference on Signals, Systems and Computers*, pages 695–699. IEEE, 2015.

[10] Giovanni Interdonato, Emil Björnson, Hien Quoc Ngo, Pål Frenger, and Erik G Larsson. Ubiquitous cell-free massive mimo communications. *EURASIP Journal on Wireless Communications and Networking*, 2019(1):197, 2019.

[11] Carmen D'Andrea, Adrian Garcia-Rodriguez, Giovanni Geraci, Lorenzo Galati Giordano, and Stefano Buzzi. Cell-free massive mimo for uav communications. In *2019 IEEE International Conference on Communications Workshops (ICC Workshops)*, pages 1–6. IEEE, 2019.

[12] Stefano Buzzi and Carmen D'Andrea. Cell-free massive mimo: User-centric approach. *IEEE Wireless Communications Letters*, 6(6):706–709, 2017.

[13] Stefano Buzzi, Carmen D'Andrea, Alessio Zappone, and Ciro D'Elia. User-centric 5g cellular networks: Resource allocation and comparison with the cell-free massive mimo approach. *IEEE Transactions on Wireless Communications*, 2019.

[14] Giovanni Interdonato, Pal Frenger, and Erik G Larsson. Utility-based downlink pilot assignment in cell-free massive mimo. In *WSA 2018; 22nd International ITG Workshop on Smart Antennas*, pages 1–8. VDE, 2018.

[15] Giovanni Interdonato, Hien Quoc Ngo, Pål Frenger, and Erik G Larsson. Downlink training in cell-free massive mimo: A blessing in disguise. *IEEE Transactions on Wireless Communications*, 18(11):5153–5169, 2019.

[16] Zheng Chen and Emil Björnson. Channel hardening and favorable propagation in cell-free massive mimo with stochastic geometry. *IEEE Transactions on Communications*, 66(11):5205–5219, 2018.

[17] Hien Quoc Ngo and Erik G Larsson. No downlink pilots are needed in tdd massive mimo. *IEEE Transactions on Wireless Communications*, 16(5):2921–2935, 2017.

[18] Giovanni Interdonato, Hien Quoc Ngo, Erik G Larsson, and Pal Frenger. How much do downlink pilots improve cell-free massive mimo? In *2016 IEEE Global Communications Conference (GLOBECOM)*, pages 1–7. IEEE, 2016.

[19] Shi Jin, Mingmei Li, Yongming Huang, Yinggang Du, and Xiqi Gao. Pilot scheduling schemes for multi-cell massive multiple-input–multiple-output transmission. *IET Communications*, 9(5):689–700, 2015.

[20] Xudong Zhu, Zhaocheng Wang, Linglong Dai, and Chen Qian. Smart pilot assignment for massive mimo. *IEEE Communications Letters*, 19(9):1644–1647, 2015.

[21] Manijeh Bashar, Kanapathippillai Cumanan, Alister G Burr, Mérouane Debbah, and Hien Quoc Ngo. On the uplink max–min sinr of cell-free massive mimo systems. *IEEE Transactions on Wireless Communications*, 18(4):2021–2036, 2019.

[22] Masoud Attarifar, Aliazam Abbasfar, and Angel Lozano. Random vs structured pilot assignment in cell-free massive mimo wireless networks. In *2018 IEEE International Conference on Communications Workshops (ICC Workshops)*, pages 1–6. IEEE, 2018.

[23] Emil Björnson and Luca Sanguinetti. A new look at cell-free massive mimo: Making it practical with dynamic cooperation. In *2019 IEEE 30th Annual International Symposium on Personal, Indoor and Mobile Radio Communications (PIMRC)*, pages 1–6. IEEE, 2019.

[24] Xudong Zhu, Linglong Dai, and Zhaocheng Wang. Graph coloring based pilot allocation to mitigate pilot contamination for multi-cell massive mimo systems. *IEEE Communications Letters*, 19(10):1842–1845, 2015.

[25] Nadisanka Rupasinghe, Yuichi Kakishima, Haralabos Papadopoulos, and Ismail Güvenç. A graph theoretic approach for training overhead reduction in fdd massive mimo systems. In *2018 IEEE International Conference on Communications (ICC)*, pages 1–7. IEEE, 2018.

[26] Hieu Trong Dao and Sunghwan Kim. Vertex graph-coloring-based pilot assignment with location-based channel estimation for massive mimo systems. *IEEE Access*, 6:4599–4607, 2018.

[27] Daewon Lee, Hanbyul Seo, Bruno Clerckx, Eric Hardouin, David Mazzarese, Satoshi Nagata, and Krishna Sayana. Coordinated multipoint transmission and reception in lte-advanced: deployment scenarios and operational challenges. *IEEE Communications Magazine*, 50(2):148–155, 2012.

[28] Jack Winters. Optimum combining for indoor radio systems with multiple users. *IEEE Transactions on communications*, 35(11):1222–1230, 1987.

[29] Soren Anderson, Mille Millnert, Mats Viberg, and Bo Wahlberg. An adaptive array for mobile communication systems. *IEEE transactions on Vehicular technology*, 40(1):230–236, 1991.

[30] Simon C Swales, Mark A Beach, David J Edwards, and Joseph P McGeehan. The performance enhancement of multibeam adaptive base-station antennas for cellular land mobile radio systems. *IEEE Transactions on Vehicular Technology*, 39(1):56–67, 1990.

[31] Erik G Larsson, Ove Edfors, Fredrik Tufvesson, and Thomas L Marzetta. Massive mimo for next generation wireless systems. *IEEE communications magazine*, 52(2):186–195, 2014.

[32] Hien Quoc Ngo. *Massive MIMO: Fundamentals and system designs*, volume 1642. Linköping University Electronic Press, 2015.

[33] Hien Quoc Ngo, Erik G Larsson, and Thomas L Marzetta. Aspects of favorable propagation in massive mimo. In *2014 22nd European Signal Processing Conference (EUSIPCO)*, pages 76–80. IEEE, 2014.

[34] Xiang Gao, Ove Edfors, Fredrik Rusek, and Fredrik Tufvesson. Linear pre-coding performance in measured very-large mimo channels. In *2011 IEEE Vehicular Technology Conference (VTC Fall)*, pages 1–5. IEEE, 2011.

[35] Hien Quoc Ngo, Erik G Larsson, and Thomas L Marzetta. Energy and spectral efficiency of very large multiuser mimo systems. *IEEE Transactions on Communications*, 61(4):1436–1449, 2013.

[36] Zhaorui Wang, Liang Liu, and Shuguang Cui. Intelligent reflecting surface assisted massive mimo communications. *arXiv preprint arXiv:2002.05899*, 2020.

[37] Antonios Pitarokoilis, Saif Khan Mohammed, and Erik G Larsson. On the optimality of single-carrier transmission in large-scale antenna systems. *IEEE Wireless Communications Letters*, 1(4):276–279, 2012.

[38] Peter Stenumgaard, Daniel Persson, Erik G Larsson, and Kia Wiklundh. An early-warning service for emerging communication problems in security and safety applications. *IEEE Communications Magazine*, 51(5):186–192, 2013.

[39] Clayton Shepard, Hang Yu, Narendra Anand, Erran Li, Thomas Marzetta, Richard Yang, and Lin Zhong. Argos: Practical many-antenna base stations. In *Proceedings of the 18th annual international conference on Mobile computing and networking*, pages 53–64, 2012.

[40] Florian Kaltenberger, Haiyong Jiang, Maxime Guillaud, and Raymond Knopp. Relative channel reciprocity calibration in mimo/tdd systems. In *2010 Future Network & Mobile Summit*, pages 1–10. IEEE, 2010.

[41] Xiang Gao, Fredrik Tufvesson, Ove Edfors, and Fredrik Rusek. Measured propagation characteristics for very-large mimo at 2.6 ghz. In *2012 Conference Record of the Forty Sixth Asilomar Conference on Signals, Systems and Computers (ASILOMAR)*, pages 295–299. IEEE, 2012.

[42] Emil Björnson, Erik G Larsson, and Thomas L Marzetta. Massive mimo: Ten myths and one critical question. *IEEE Communications Magazine*, 54(2):114–123, 2016.

[43] Xiang Gao, Ove Edfors, Fredrik Rusek, and Fredrik Tufvesson. Massive mimo performance evaluation based on measured propagation data. *IEEE Transactions on Wireless Communications*, 14(7):3899–3911, 2015.

[44] Jubin Jose, Alexei Ashikhmin, Thomas L Marzetta, and Sriram Vishwanath. Pilot contamination and precoding in multi-cell tdd systems. *IEEE Transactions on Wireless Communications*, 10(8):2640–2651, 2011.

[45] Emil Björnson, Erik G Larsson, and Merouane Debbah. Massive mimo for maximal spectral efficiency: How many users and pilots should be allocated? *IEEE Transactions on Wireless Communications*, 15(2):1293–1308, 2015.

[46] Shlomo Shamai and Benjamin M Zaidel. Enhancing the cellular downlink capacity via co-processing at the transmitting end. In *IEEE VTS 53rd Vehicular Technology Conference, Spring 2001. Proceedings (Cat. No. 01CH37202)*, volume 3, pages 1745–1749. IEEE, 2001.

[47] Shidong Zhou, Ming Zhao, Xibin Xu, Jing Wang, and Yan Yao. Distributed wireless communication system: a new architecture for future public wireless access. *IEEE Communications Magazine*, 41(3):108–113, 2003.

[48] Sivarama Venkatesan, Angel Lozano, and Reinaldo Valenzuela. Network mimo: Overcoming intercell interference in indoor wireless systems. In *2007 Conference Record of the Forty-First Asilomar Conference on Signals, Systems and Computers*, pages 83–87. IEEE, 2007.

[49] Giuseppe Caire, Sean A Ramprashad, and Haralabos C Papadopoulos. Rethinking network mimo: Cost of csit, performance analysis, and architecture comparisons. In *2010 Information Theory and Applications Workshop (ITA)*, pages 1–10. IEEE, 2010.

[50] David Gesbert, Stephen Hanly, Howard Huang, Shlomo Shamai Shitz, Osvaldo Simeone, and Wei Yu. Multi-cell mimo cooperative networks: A new look at interference. *IEEE journal on selected areas in communications*, 28(9):1380–1408, 2010.

[51] Mauro Boldi, Antti Tölli, Magnus Olsson, Eric Hardouin, Tommy Svensson, Federico Boccardi, Lars Thiele, and Volker Jungnickel. Coordinated multipoint (comp) systems. *Mobile and Wireless Communications for IMT-Advanced and Beyond*, pages 121–155, 2011.

[52] Afif Osseiran, Jose F Monserrat, and Patrick Marsch. *5G mobile and wireless communications technology*. Cambridge University Press, 2016.

[53] Elina Nayebi, Alexei Ashikhmin, Thomas L Marzetta, Hong Yang, and Bhaskar D Rao. Precoding and power optimization in cell-free massive mimo systems. *IEEE Transactions on Wireless Communications*, 16(7):4445–4459, 2017.

[54] Emil Bjornson, Randa Zakhour, David Gesbert, and Björn Ottersten. Cooperative multicell precoding: Rate region characterization and distributed strategies with instantaneous and statistical csi. *IEEE Transactions on Signal Processing*, 58(8):4298–4310, 2010.

[55] Giovanni Interdonato, Hien Quoc Ngo, Erik G Larsson, and Pal Frenger. How much do downlink pilots improve cell-free massive mimo? In *2016 IEEE Global Communications Conference (GLOBECOM)*, pages 1–7. IEEE, 2016.

[56] Steven M Kay. *Fundamentals of statistical signal processing*. Prentice Hall PTR, 1993.

[57] Sassan Ahmadi. *LTE-Advanced: a practical systems approach to understanding 3GPP LTE releases 10 and 11 radio access technologies*. Academic Press, 2013.

[58] Hien Quoc Ngo, Le-Nam Tran, Trung Q Duong, Michail Matthaiou, and Erik G Larsson. On the total energy efficiency of cell-free massive mimo. *IEEE Transactions on Green Communications and Networking*, 2(1):25–39, 2017.

[59] Manijeh Bashar, Kanapathippillai Cumanan, Alister G Burr, Merouane Debbah, and Hien Quoc Ngo. On the uplink max-min sinr of cell-free massive mimo systems. *IEEE Transactions on Wireless Communications*, pages 1–1, 2019.

[60] Hamed Ahmadi, Arman Farhang, Nicola Marchetti, and Allen MacKenzie. A game theoretic approach for pilot contamination avoidance in massive mimo. *IEEE Wireless Communications Letters*, 5(1):12–15, 2015.

[61] Ramiz Sabbagh, Cunhua Pan, and Jiangzhou Wang. Pilot allocation and sum-rate analysis in cell-free massive mimo systems. In *2018 IEEE International Conference on Communications (ICC)*, pages 1–6. IEEE, 2018.

[62] Emil Björnson and Luca Sanguinetti. Scalable cell-free massive mimo systems. *IEEE Transactions on Communications*, 2020.

[63] Rhyd Lewis. *A guide to graph colouring*, volume 7. Springer, 2015.

[64] Yuvraj Singh. Comparison of okumura, hata and cost-231 models on the basis of path loss and signal strength. *International journal of computer applications*, 59(11), 2012.

[65] M Vanidevi and N Selvaganesan. Channel estimation for finite scatterers massive multi-user mimo system. *Circuits, Systems, and Signal Processing*, 36(9):3761–3777, 2017.

[66] Thong T Do, Lu Gan, Nam H Nguyen, and Trac D Tran. Fast and efficient compressive sensing using structurally random matrices. *IEEE Transactions on signal processing*, 60(1):139–154, 2011.

[67] Xudong Zhu, Linglong Dai, Zhaocheng Wang, and Xiaodong Wang. Weighted-graph-coloring-based pilot decontamination for multicell massive mimo systems. *IEEE Transactions on Vehicular Technology*, 66(3):2829–2834, 2016.

[68] Wafa Haj Hmida, Vahid Meghdadi, Ammar Bouallegue, and Jean Pierre Cances. Graph coloring based pilot reuse among interfering users in cell-free massive mimo. In *ICC*, 2020.

[69] Zakir Hussain Shaik, Emil Björnson, and Erik G Larsson. Cell-free massive mimo with radio stripes and sequential uplink processing. *arXiv*, pages arXiv–2003, 2020.

[70] Ertugrul Basar. Transmission through large intelligent surfaces: A new frontier in wireless communications. In *2019 European Conference on Networks and Communications (EuCNC)*, pages 112–117. IEEE, 2019.

[71] Jesus Rodriguez Sanchez, Ove Edfors, Fredrik Rusek, and Liang Liu. Processing distribution and architecture tradeoff for large intelligent surface implementation. *arXiv preprint arXiv:2001.04937*, 2020.

[72] Ertugrul Basar, Marco Di Renzo, Julien De Rosny, Merouane Debbah, Mohamed-Slim Alouini, and Rui Zhang. Wireless communications through reconfigurable intelligent surfaces. *IEEE Access*, 7:116753–116773, 2019.

[73] Özgecan Özdogan, Emil Björnson, and Erik G Larsson. Intelligent reflecting surfaces: Physics, propagation, and pathloss modeling. *IEEE Wireless Communications Letters*, 2019.

[74] Emil Björnson, Özgecan Özdogan, and Erik G Larsson. Intelligent reflecting surface vs. decode-and-forward: How large surfaces are needed to beat relaying? *IEEE Wireless Communications Letters*, 2019.

[75] Mehrdad Khani, Mohammad Alizadeh, Jakob Hoydis, and Phil Fleming. Adaptive neural signal detection for massive mimo. *IEEE Transactions on Wireless Communications*, 2020.

[76] Emil Björnson, Luca Sanguinetti, Henk Wymeersch, Jakob Hoydis, and Thomas L Marzetta. Massive mimo is a reality—what is next?: Five promising research directions for antenna arrays. *Digital Signal Processing*, 94:3–20, 2019.

[77] Emil Björnson, Özgecan Özdogan, and Erik G Larsson. Reconfigurable intelligent surfaces: Three myths and two critical questions. *arXiv preprint arXiv:2006.03377*, 2020.

[78] Nandana Rajatheva, Italo Atzeni, Emil Bjornson, Andre Bourdoux, Stefano Buzzi, Jean-Baptiste Dore, Serhat Erkucuk, Manuel Fuentes, Ke Guan, Yuzhou Hu, et al. White paper on broadband connectivity in 6g. *arXiv preprint arXiv:2004.14247*, 2020.